

Conserved N-terminal cysteine dioxygenases transduce responses to hypoxia in animals and plants

Norma Masson^{1,*}, Thomas P. Keeley^{1,*}, Beatrice Giuntoli^{3,4*}, Mark D. White^{2,*}, Mikel Lavilla Puerta⁴, Pierdomenico Perata⁴, Richard J. Hopkinson², Emily Flashman^{2,a}, Francesco Licausi^{3,4,a}, Peter J. Ratcliffe^{1,5,a**}

¹Ludwig Institute for Cancer Research, Nuffield Department of Medicine, University of Oxford, Oxford OX3 7FZ, UK

²Chemistry Research Laboratory, University of Oxford, Mansfield Road, Oxford OX1 3TA, UK

³Department of Biology, University of Pisa, Via Luca Ghini 13, Pisa 56126, Italy

⁴Plantlab, Institute of Life Sciences, Scuola Superiore Sant'Anna, Via Guidiccioni 8/10, Pisa 56124, Italy

⁵The Francis Crick Institute, 1 Midland Road, London NW1 1AT, UK

*Joint first authors, ^a Joint senior authors

**Corresponding author. Email: peter.ratcliffe@ndm.ox.ac.uk

Abstract

Organisms must respond to hypoxia to preserve oxygen homeostasis. We identify a thiol oxidase, previously assigned as cysteamine (2-aminoethanethiol) dioxygenase (ADO), as a high K_m O₂ N-terminal cysteine dioxygenase that transduces the oxygen-regulated stability of proteins by the N-degron pathway in human cells. ADO catalyzes conversion of N-terminal cysteine to cysteine sulfinic acid and is related to the plant cysteine oxidases that mediate responses to hypoxia by an identical post-translational modification. In human cells we show that ADO regulates the RGS4/5 (regulator of G-protein signalling) N-degron substrates, modulates G-protein coupled Ca²⁺ signals and MAPK (mitogen-activated protein kinase) activity, and that its activity extends to other N-Cysteine proteins including the angiogenic cytokine IL-32. Identification of a conserved enzymatic oxygen sensor in multicellular eukaryotes opens routes to better understanding and therapeutic targeting of adaptive responses to hypoxia.

Oxygen homeostasis is critical for most forms of life, and is impaired in most human diseases. Previous work identified the hypoxia inducible factor (HIF) prolyl hydroxylases as human oxygen sensors(1). These regulatory enzymes are 2-oxoglutarate (2-OG) dependent dioxygenases, with high K_mO_2 values, which catalyze *trans*-4-prolyl hydroxylation of the transcription factor HIF(2, 3), to target it for proteolysis. Hence they regulate a broad range of transcriptional responses to hypoxia (reviewed in(4)). Although the prolyl hydroxylation of HIF was unprecedented as a signaling system, subsequent work has revealed different systems of enzymatic protein oxidation, which signal hypoxia in representatives of all four eukaryotic kingdoms (5-7). In each system the protein oxidation event is linked to protein degradation.

Of particular interest is the Cys-branch of the N-degron pathway(8). Following the action of methionine aminopeptidases, oxidation of N-terminal cysteines creates a substrate for arginyl-transferases, which catalyze addition of this N-terminal destabilizing residue, promoting degradation. No cysteine-modifying enzyme was defined, but N-terminal cysteine oxidation was shown to be affected by nitric oxide (9), and based on *in vitro* studies, cysteine oxidation has been considered likely to be non-enzymatic. Subsequently, in plants, it was shown that the Cys-branch of the N-degron pathway controls the stability of ethylene response transcription factors (ERF-VII) (10, 11). Further studies in *Arabidopsis thaliana* revealed that Cys-oxidation is catalyzed by a series of plant cysteine oxidases (PCOs), which act as oxygen sensors directing hypoxic adaptation (7, 12). These findings led us to further investigate the mechanism of N-terminal cysteine oxidation in animals.

First, we created human osteosarcoma U-2OS and colon cancer RKO cells that stably express a fusion protein comprising N-terminal sequences that are sufficient for oxygen-dependent degradation of the ERF-VII transcription factor RAP2.12 (Related to APETALA2) in plants, linked to a GFP:V5 reporter, and exposed these cells to hypoxia. To distinguish responses from those transduced by HIF, we also tested known inhibitors of the HIF prolyl hydroxylases that differ in their specificity both for other iron-dependent dioxygenases and non-enzymatic metal catalysed oxidation. Exposure of the transfected cells to hypoxia and to the non-specific iron chelator, dipyrindyl, resulted in accumulation of the RAP₁₋₅₀:GFP:V5 reporter protein, but not that of a C2A mutant, without affecting reporter

transcript levels (fig. S1). In contrast, neither reporter was activated by non-specific 2-OG dioxygenase inhibitors (DFO and DMOG), or a HIF prolyl hydroxylase inhibitor (PHI), all of which robustly induced HIF (Fig. 1A). For cells exposed to hypoxia for 16 h, then treated with cycloheximide, before being re-oxygenated or maintained in hypoxia, we found that hypoxia prolonged the reporter protein half-life from ~5 to 35 min (Fig. 1B and fig. S2). These findings demonstrated an iron and oxygen-dependent activity in human cells that is distinct from the HIF prolyl hydroxylases and that operates in a Cys2-dependent manner on amino-acid sequences from plant RAP2.12.

We next compared this response with that of members of the R4 group of RGS proteins, which are targets of the Cys-branch of the N-degron pathway in humans and mice (13, 14). Experiments on RKO cells stably expressing HA-tagged RGS4 (RGS4:HA) and an RGS4:GFP fusion (RGS4₁₋₂₀:GFP), each encoding wild-type or C2A mutant sequences, revealed accumulation of wild-type, but not mutant proteins in cells exposed to hypoxia and dipyridyl, but not DMOG or DFO (Fig. 1C and fig. S3). Endogenous RGS4 and RSG5 proteins in human neuroblastoma SH-SY5Y cells responded identically to the same set of compounds (Fig. 1D). Responses of these RGS proteins to graded hypoxia were further examined in a series of human (SH-SY5Y, RKO, human endothelial EA.hy926) and mouse embryonic sarcoma (C3H/10T1/2) cells, revealing progressive accumulation of RGS4 or RGS5 proteins in response to physiological hypoxia (Fig. 1E and fig. S4). These changes were observed at the level of proteins and not mRNAs, with the exception of RGS4 in SH-SY5Y. Thus, plant and human reporter proteins and endogenous RGS proteins appeared to be regulated similarly, suggesting that human cells might regulate their stability using enzyme(s) similar to the PCOs.

The human genome contains two thiol dioxygenases with similar predicted structure to the PCOs, cysteine dioxygenase (CDO1) and an enzyme previously assigned as cysteamine (2-aminoethanethiol) dioxygenase (ADO) (15, 16). Genes encoding these enzymes and PCO1 were co-transfected with the RGS4:HA gene into human embryonic kidney 293T cells. Overexpressed ADO, but not CDO1, suppressed hypoxic induction of RGS4:HA, in a manner dependent on cysteine at position 2 (Fig. 2A). At these levels of overexpression, RGS4:HA was not suppressed by PCO1. The ability of ADO

to suppress RGS4:HA was inhibited by combined exposure to hypoxia and dipyridyl and ablated by H112A+H114A mutations (fig. S5) that prevent assembly of the catalytic iron center (15). These experiments indicated that the catalytic activity of overexpressed ADO was sufficient to suppress RGS4:HA.

We next inactivated ADO and CDO1 in SH-SY5Y and RKO cells, using CRISPR/Cas9-mediated gene editing. Inactivation of ADO but not CDO1 led to constitutive upregulation of endogenous and transfected RGS4 and RGS5 proteins irrespective of oxygen levels (Fig. 2B and figs. S6, S7). In view of reported actions of nitric oxide on RGS proteins (9, 17), we also tested responses to the nitric oxide donor DETA-NO in wild type and ADO-deficient cells. Suppression of hypoxic RGS4 levels by DETA-NO in wild-type SH-SY5Y and RKO cells was also abrogated in ADO-deficient cells (fig. S8). Stable re-expression of ADO, but not overexpression of CDO1, suppressed levels of RGS proteins (figs. S7 and S9). Under these conditions, expression of PCO1 also suppressed RGS proteins and restored regulation by oxygen, demonstrating oxygen-dependent activity of the plant enzyme on endogenous human proteins. In SH-SY5Y cells, we then inactivated the arginyl-transferase ATE1 that operates downstream of the proposed Cys-oxidation in the N-degron pathway. Up-regulation of RGS5 in ATE1-deficient and ADO-deficient cells was similar, and was not suppressed by overexpression of ADO in ATE1-deficient cells (Fig. 2C). Thus ADO is required for oxygen-dependent degradation of RGS proteins. This activity was dependent on the integrity of ATE1, consistent with ADO acting upstream of ATE1 in the N-degron pathway.

To explore whether ADO can complement deficient PCO in plants, we generated a PCO-depleted *Arabidopsis thaliana* mutant by crossing plants in which four of the five known PCO (1, 2, 4 and 5) genes were inactivated by T-DNA insertional mutagenesis. Homozygous quadruple *pco1/2/4/5* mutant plants (*4pco*), but not triple *pco1/2/4* (*3pco*), manifested severe developmental defects (Fig. 2D) and upregulation of hypoxia-responsive genes under aerobic conditions (Fig. 2E). When human ADO, but not CDO1, was introduced into *4pco* plants under control of the PCO1 promoter, the constitutive upregulation of anaerobic genes in air was corrected and the plants developed normally (Figs. 2D and 2E, and fig. S10). Consistent with complementation of defective PCO function, co-expression of

ADO in *A. thaliana* protoplasts caused dose-dependent suppression of RAP2.12 luciferase fusion protein activity (fig. S10).

Interestingly, in budding yeast, Cys is not a destabilizing N-terminal residue (18). To determine if deficiency of an ADO-like enzyme might be responsible for the stability associated with N-Cys in yeast, we introduced ADO or CDO1 into yeast cells together with a ratio-metric reporter in which the activity of a RAP2.12-Firefly Luciferase fusion protein or a C2A mutant is normalized to Renilla Luciferase (fig. S11). Expression of human ADO but not CDO1 reduced the activity of, and conferred hypoxic regulation on, the RAP₂₋₂₈-FLuc protein but not a C2A mutant (Fig. 2F and fig. S11). Consistent with this, phylogenetic analyses revealed potential ADO/CDO orthologues across most plants, animals and at least some protist species, but not fungi (fig. S12). Together, these findings explain the lack of activity of cysteine as a destabilizing residue in yeast, but suggest the pathway might otherwise operate widely in eukaryotic species.

Cross-complementation suggested that ADO catalyzes a form of N-terminal cysteine dioxygenation similar to that catalyzed by the PCOs. To test this, we produced recombinant human ADO and CDO1 in *E. coli*, reacted these enzymes with synthetic peptides corresponding to residues 2-15 of human RGS4 and RGS5 and examined the products by mass spectrometry. We found that the peptides were modified by +32 Da mass addition by ADO but not CDO1 (Fig. 3A and fig. S13) and that this modification was suppressed in anaerobic conditions (Fig. 3B). To confirm dioxygenation, we conducted the reactions in an atmosphere of ¹⁸O₂ or in the presence of ¹⁸O-labelled water (H₂¹⁸O). These experiments revealed a single +36 Da mass addition in ¹⁸O₂, and a single +32 Da mass addition in the presence of ¹⁸O-labelled water, demonstrating that two oxygen atoms were incorporated directly into the peptide from molecular oxygen and confirming dioxygenation (Fig. 3B). MS2 assigned the modification to the N-terminal cysteine (fig. S14). Thus, human ADO catalyzes the dioxygenation of N-Cys residues in RGS4 and RGS5 to cysteine sulfinic acid. Kinetic measurements on human ADO (Fig. 3C and fig. S15) revealed high k_{catPep} values of 20.1 and 16.9 s⁻¹ on RGS4 and RGS5 peptides under atmospheric conditions, but marked sensitivity to oxygen ($K_mO_2^{app} > 500$ μM). Thus ADO resembles the HIF prolyl hydroxylase enzymes in manifesting a K_mO_2 that is significantly above the

physiological range, a property that may underpin a role in oxygen homeostasis. Given the original assignment of ADO as cysteamine dioxygenase we also examined for competition of N-Cys peptide dioxygenation by free cysteamine and cysteine, but found inhibition only at high concentrations of these metabolites (IC₅₀ 37 and 13mM, respectively, fig. S16).

RGS4 and RGS5 regulate heterotrimeric G-protein signaling by enhancing G α -coupled GTP hydrolysis and hence attenuating G-protein signals. Since the catalytic activity of ADO lowers levels of RGS4 and 5, ADO-deficient cells in which levels of these proteins are increased, should manifest attenuation of G-protein signaling on relevant pathways. G α proteins can regulate the activity of mitogen-activated protein kinase (MAPK) pathways (14, 19). Consistent with this, mouse cells and embryos with a defective N-degron pathway due to loss of the arginyl-transferase ATE1, have been shown to exhibit reduced activation of MAPK kinase (14). We therefore assayed phosphorylation of MAPK (p44/p42) in ADO-deficient SH-SY5Y cells (Fig. 4A). These experiments revealed reduced levels of phosphorylated MAPK in ADO-deficient SH-SY5Y cells that were similar to levels of phosphorylated p44/p42 in ATE1-deficient SH-SY5Y cells. Reduction in phosphorylated p44/p42 was reversed by expression of ADO in ADO KO but not ATE1 KO cells (Fig. 4B). To test the effects of ADO on responses to a specific G-protein coupled agonist, we examined carbachol, a cholinergic agonist whose muscarinic receptor is coupled via G α_q to the regulation of intracellular Ca²⁺. Attenuation of Ca²⁺ mobilization in response to carbachol (Fig. 4C), but not the receptor-independent ionophore, ionomycin (Fig. 4D), was observed in ADO-deficient cells and was reversed by re-expression of ADO. Given the complexity of interactions among RGS proteins and G-protein signaling pathways, we cannot be certain that these effects are entirely caused by effects of ADO on RGS4 and RGS5 proteins. Nevertheless, the work establishes a role for ADO in the regulation G-protein signaling, consistent with its role as a Cys-modifying enzyme in the N-degron pathway regulating RGS proteins.

N-terminal sequence analyses of proteins encoded by plant and animal genomes have suggested the existence of many other potential substrates for the Cys-branch of the N-degron pathway (7, 9) and ADO is more widely expressed in human cells and tissues than RGS4/5(20). We therefore sought to

determine whether ADO-mediated oxygen-dependent regulation of human proteins extended beyond the identified RGS proteins. To pursue this, we first reacted recombinant ADO with a diverse series of peptides derived from proteins predicted to be processed to generate N-Cys polypeptides, and monitored for dioxygenation (+32 Da mass shift) by MS. These experiments revealed substrate-dependent catalytic activity of ADO, ranging from close to zero, to levels that were similar to those using RGS5 peptide (figs. S17, S18). We then examined endogenous protein levels corresponding to peptide substrates that supported high (IL-32, Fig. 5A) or very low (asparagine synthetase, (ASNS) and JunB) ADO-catalyzed dioxygenation using available antibodies. These experiments were conducted in the previously engineered ADO-deficient RKO cells as IL-32 was not detected in SH-SY5Y cells. Immunoblotting revealed that the abundance of IL-32, but not ASNS or JunB, was increased in hypoxic cells, accumulated constitutively in ADO-deficient cells and was reduced by re-expression of transfected ADO (Fig. 5B). Experiments in wild type and ADO-deficient RKO cells confirmed IL-32 regulation at the protein but not mRNA level (Fig. 5C). Further experiments confirmed dioxygenation of the N-terminal cysteine following reaction of the IL-32 peptide with recombinant ADO (fig. S18), and that this residue was necessary for ADO-mediated suppression of co-transfected IL-32 in cells (Fig. 5D). These findings demonstrate that ADO target proteins do extend beyond RGS proteins and identify human IL-32 as one such protein. The tested peptides represent only a small fraction of N-Cys polypeptides that might be generated in cells and it is therefore likely that other ADO-regulated human targets exist. Interestingly, the transcriptional regulator LITTLE ZIPPER 2 and a component of Polycomb Repressor 2 Complex, VERNALIZATION 2, have recently been identified as new oxygen-regulated targets of the N-degron pathway in plants(21, 22). Given the emerging complexity of N-degron regulation(8), in which other processes may compete with ADO-catalysed deoxygenation, it cannot be assumed that high levels of ADO-catalysis on isolated peptides will necessarily predict physiological regulation by ADO, or indeed that all protein regulation by ADO operates through the same downstream pathways. Identification of human ADO as an enzymatic human oxygen sensor should open the way to understanding responses to hypoxia that are transduced by these pathways.

Conservation of ADO and the PCOs as human and plant oxygen sensors contrasts with the absence of conservation of their known substrates, and with different challenges to oxygen homeostasis that are encountered by animals and plants. In plants, the ERF-VII pathway directs transcriptional responses to hypoxia that require time for the transcriptional output to engage adaptive responses. In animal cells the principal process regulating transcriptional responses to hypoxia is the prolyl hydroxylation of HIF. In contrast, direct operation of ADO on the protein stability of signaling molecules has the potential to transduce more rapid responses to hypoxia than HIF. RGS4 and RGS5 have been implicated in oxygen homeostasis in mammals through effects on the cardiovascular system and angiogenesis(13, 19, 23). IL-32 is an atypical cytokine that regulates pro-inflammatory cytokine networks and angiogenic growth factors(24, 25). Although our findings identify ADO as an essential regulator of responses of these proteins to hypoxia, it is of interest that RGS4, RGS5 and IL-32 have all been reported to be transcriptional targets of HIF(26-28). Consistent with the reported cell-type specific regulation of RGS4 by HIF(26), we did observe induction of RGS4 mRNA by hypoxia in SH-SY5Y, but not other cells. These findings predict that in specific cellular settings where both systems are operative the ADO and HIF prolyl hydroxylase systems will interact to generate physiological responses to hypoxia. In conclusion, our work defines an enzymatic human oxygen sensor, most likely operating physiologically on a shorter time scale than the transcriptional responses transduced by the HIF prolyl hydroxylases and opens a new route to the investigation of adaptive responses to hypoxia, potentially including their therapeutic augmentation by catalytic inhibitors of ADO.

References

1. A. C. R. Epstein *et al.*, *C. elegans* EGL-9 and mammalian homologues define a family of dioxygenases that regulate HIF by prolyl hydroxylation. *Cell* **107**, 43-54 (2001).
2. M. Ivan *et al.*, HIF α targeted for VHL-mediated destruction by proline hydroxylation: implications for O₂ sensing. *Science* **292**, 464-468 (2001).
3. P. Jaakkola *et al.*, Targeting of HIF- α to the von Hippel-Lindau ubiquitylation complex by O₂-regulated prolyl hydroxylation. *Science* **292**, 468-472 (2001).
4. W. G. J. Kaelin, P. J. Ratcliffe, Oxygen sensing by metazoans: The central role of the HIF hydroxylase pathway. *Molecular Cell* **30**, 393-402 (2008).
5. C. M. West, H. van der Wel, Z. A. Wang, Prolyl 4-hydroxylase-1 mediates O₂ signaling during development of Dictyostelium. *Development* **134**, 3349-3358 (2007).

6. B. T. Hughes, P. J. Espenshade, Oxygen-regulated degradation of fission yeast SREBP by Ofd1, a prolyl hydroxylase family member. *EMBO Journal* **27**, 1491-1501 (2008).
7. D. A. Weits *et al.*, Plant cysteine oxidases control the oxygen-dependent branch of the N-end-rule pathway. *Nature communications* **5**, 3425 (2014).
8. A. Varshavsky, N-degron and C-degron pathways of protein degradation. *Proceedings of the National Academy of Sciences of the United States of America* **116**, 358-366 (2019).
9. R. G. Hu *et al.*, The N-end rule pathway as a nitric oxide sensor controlling the levels of multiple regulators. *Nature* **437**, 981-986 (2005).
10. F. Licausi *et al.*, Oxygen sensing in plants is mediated by an N-end rule pathway for protein destabilization. *Nature* **479**, 419-422 (2011).
11. D. J. Gibbs *et al.*, Homeostatic response to hypoxia is regulated by the N-end rule pathway in plants. *Nature* **479**, 415-418 (2011).
12. M. D. White *et al.*, Plant cysteine oxidases are dioxygenases that directly enable arginyl transferase-catalysed arginylation of N-end rule targets. *Nature communications* **8**, 14690 (2017).
13. Y. T. Kwon *et al.*, An essential role of N-terminal arginylation in cardiovascular development. *Science* **297**, 96-99 (2002).
14. M. J. Lee *et al.*, RGS4 and RGS5 are in vivo substrates of the N-end rule pathway. *Proc Natl Acad Sci U S A* **102**, 15030-15035 (2005).
15. J. E. Dominy, Jr. *et al.*, Discovery and characterization of a second mammalian thiol dioxygenase, cysteamine dioxygenase. *J Biol Chem* **282**, 25189-25198 (2007).
16. M. H. Stipanuk, C. R. Simmons, P. A. Karplus, J. E. Dominy, Jr., Thiol dioxygenases: unique families of cupin proteins. *Amino Acids* **41**, 91-102 (2011).
17. I. M. Jaba *et al.*, NO triggers RGS4 degradation to coordinate angiogenesis and cardiomyocyte growth. *J Clin Invest* **123**, 1718-1731 (2013).
18. A. Varshavsky, The N-end rule. *Cell* **69**, 725-735 (1992).
19. C. Arnold *et al.*, Hypertension-evoked RhoA activity in vascular smooth muscle cells requires RGS5. *FASEB J* **32**, 2021-2035 (2018).
20. M. Uhlen *et al.*, Proteomics. Tissue-based map of the human proteome. *Science* **347**, 1260419 (2015).
21. D. A. Weits *et al.*, An apical hypoxic niche sets the pace of shoot meristem activity. *Nature* **569**, 714-717 (2019).
22. D. J. Gibbs *et al.*, Oxygen-dependent proteolysis regulates the stability of angiosperm polycomb repressive complex 2 subunit VERNALIZATION 2. *Nature communications* **9**, 5438 (2018).
23. J. Hamzah *et al.*, Vascular normalization in Rgs5-deficient tumours promotes immune destruction. *Nature* **453**, 410-414 (2008).
24. C. A. Nold-Petry *et al.*, IL-32 promotes angiogenesis. *Journal of immunology* **192**, 589-602 (2014).
25. Y. J. E. Slood, J. W. Smit, L. A. B. Joosten, R. T. Netea-Maier, Insights into the role of IL-32 in cancer. *Semin Immunol* **38**, 24-32 (2018).
26. S. W. Olechnowicz, A. O. Fedele, D. J. Peet, Hypoxic induction of the regulator of G-protein signalling 4 gene is mediated by the hypoxia-inducible factor pathway. *PLoS One* **7**, e44564 (2012).
27. Y. Jin *et al.*, RGS5, a hypoxia-inducible apoptotic stimulator in endothelial cells. *J Biol Chem* **284**, 23436-23443 (2009).
28. M. Zahoor *et al.*, Hypoxia promotes IL-32 expression in myeloma cells, and high expression is associated with poor survival and bone loss. *Blood Adv* **1**, 2656-2666 (2017).
29. M. L. Puerta *et al.*, A Ratiometric Sensor Based on Plant N-Terminal Degrons Able to Report Oxygen Dynamics in *Saccharomyces cerevisiae*. *J Mol Biol*, (2019).

Acknowledgements

We thank J. Riepsaame for help with the creation of CRISPR/Cas9-edited cell lines, K. Buckler for guidance in Ca^{2+} measurements, E. Pires for mass spectrometry advice, G. Novi for crossing *A thaliana PCO* mutants, and V. Shukla for help with yeast transformation.

Funding: The work was supported by the Ludwig Institute for Cancer Research, the Wellcome Trust (grant number 106241/Z/14/Z), Scuola Superiore Sant'Anna and Biotechnology and Biological Research Council (UK) New Investigator Grant BB/M024458/1. This work was also supported by the Francis Crick Institute, which receives its core funding from Cancer Research UK (FC001501), the UK Medical Research Council (FC001501), and the Wellcome Trust (FC001501). B. Giuntoli was supported by the EMBO short-term fellowship 7233.

Author contributions: PJR, FL and EF conceived the experiments; NM, TPK, BG, MDW, MLP, PP, RJH designed and performed the experiments. PJR, FL, EF, NM, TK, BG and MDW wrote the manuscript.

Competing interests: PJR is a scientific co-founder holds equity in Reox Ltd, has served on the Research Advisory Board of GSK Ltd., and is co-inventor on patents disclosing methods and means of assaying for HIF hydroxylases inhibitors and their use in the treatment of hypoxic diseases (US8535899, EP1379630), which have been licensed to Reox Ltd. PJR, FL, EF, NM, TK, BG, MDW are inventors on a patent application related to this work (United Kingdom Patent Application No. 1908332.8). The other authors declare no competing interests.

Data and materials availability

All data is available in the manuscript or the supplementary materials.

List of Supplementary materials:

Materials and Methods

Fig S1 – S18

Reference 29.

Figure Legends

Fig. 1. Regulation of plant and animal N-degron substrates by oxygen in human cells. (A) Levels of fusion proteins linking the N-terminal 1-50 residues of plant RAP2.12 or a C2A mutant to a GFP:V5 cassette (RAP₁₋₅₀:V5; RAP₁₋₅₀(C2A):V5) in stably transfected U-2OS cells exposed to hypoxia or the indicated inhibitors. (B) RAP₁₋₅₀:V5 reporter protein half-life in cells incubated in hypoxia (16 h, 1% O₂) then treated with cycloheximide (100 μM, 10min), then maintained in hypoxia or re-oxygenated for the indicated times. (C) C-terminal hemagglutinin (HA) tagged human RGS4, (RGS4:HA) or a C2A mutant in stably transfected RKO cells exposed to hypoxia or inhibitors. (D and E) Endogenous RGS4 and RGS5 proteins in SH-SY5Y cells exposed to inhibitors (D) or graded hypoxia (E). Similar patterns of response were observed for the plant fusion-protein reporter, transfected RGS4:HA and endogenous RGS4/5 proteins; responses of exogenous proteins were abolished by C2A mutation. 2,2 DIP, 2,2-dipyridyl (100 μM); DFO, desferrioxamine (100 μM); DMOG, dimethyloxalylglycine (1 mM); PHI, prolyl hydroxylase inhibitor (125 μM); MG132, proteasomal inhibitor (25 μM). All exposures of cells to hypoxia or inhibitors were for 4 h unless otherwise indicated. In panel A HIF-1α immunoblots are provided for comparison.

Fig. 2. ADO controls the oxygen dependent Cys-branch of the N-degron pathway. (A) RGS4:HA and RGS4(C2A):HA protein levels in 293T cells after co-expression with either control (EV), ADO, CDO1 or PCO1. Cells were exposed to hypoxia (0.5% O₂, 16 h) or maintained in air. Comparable enzyme levels were confirmed by separate FLAG-immunoblotting. (B) Endogenous RGS4 and RGS5 proteins in ADO-deficient SH-SY5Y cells (ADO KO); RGS4 and RGS5 are constitutive and insensitive to iron chelators or hypoxia. (C) Over-expression of ADO does not repress constitutive stabilization of RGS5 in ATE1-deficient (ATE1 KO) cells. (D) Expression of human ADO restores wild type phenotype in *4pco A. thaliana* mutants; *3pco* mutants which did not manifest this phenotype were unaffected by ADO. (E) Box plots showing relative mRNA level of hypoxia-inducible genes in wild type and *pco* mutant plants that express ADO. ADO significantly reduced expression of the hypoxia-inducible genes *PDC1*, *ADH*, *LBD41* and *SAD6* in *4pco* mutants, Mean ± S.D. *P<0.05;

Mann-Whitney Rank Sum Test) with levels of non-hypoxia-inducible genes unchanged (fig. S10). (F) Relative luciferase activity (Fluc/Rluc) in *S. cerevisiae* cells expressing C-DLOR (Cys) or A-DLOR (Cys to Ala mutant) reporter under aerobic and hypoxic conditions in the presence or absence of human ADO or CDO1, mean \pm S.D. * $P < 0.05$; 2-way ANOVA followed by Holm-Sidak post hoc test.

Fig. 3. ADO catalyzes the dioxygenation of the N-terminal Cys of RGS4/5 peptides. (A) MS spectra show a mass shift of +32 Da when RGS5 N-terminal peptide was incubated with recombinant human ADO, but not with recombinant human CDO1. Similar results were obtained when an RGS4 N-terminal peptide was used (fig. S13). (B) The ADO-catalyzed +32 Da mass addition is absent when reactions were conducted under anaerobic (100% N_2) conditions; ^{18}O labelling demonstrates incorporation of 2 oxygen atoms derived directly from molecular O_2 and not H_2O . (C) Summary table of reaction kinetics for ADO-catalyzed dioxygenation of N-terminal RGS4/5 peptides. The influence of varying peptide concentration under atmospheric conditions (k_{cat}^{Pep} and $K_m^{Pep^{app}}$) and O_2 levels using a fixed, non-limiting concentration of peptide ($k_{cat}^{O_2}$ and $K_m^{O_2^{app}}$) were examined to determine sensitivities to both substrates. Source data are in fig. S15.

Fig. 4. ADO regulates G-protein signalling. (A-D) ADO regulates G-protein signalling in SH-SY5Y cells. (A) MAPK (p44/42) phosphorylation in WT, ADO KO and ATE1 KO cells. Immunoblot lanes represent separate biological replicates, with densitometric analysis provided below. Mean \pm S.D. $n=3$, *** $P < 0.001$ one-way ANOVA with Holm-Sidak post hoc test. (B) Re-expression of ADO increases phosphorylated p44/42 in ADO KO, but not ATE1 KO cells, mean \pm S.D. $n=3$, ** $P < 0.01$ two-way ANOVA with Holm-Sidak post hoc test. (C) Carbachol (CCh) stimulated rises in $[Ca^{2+}]_i$ are attenuated in ADO-deficient (KO) compared with wild-type (WT) cells. A representative trace is provided and mean peak change in R405/495 intensity at each CCh concentration is shown (inset). $n=8-12$, *** $P < 0.001$, 3-parameter non-linear regression analysis. (D) Ionomycin ($0.1\mu M$) is equipotent at stimulating Ca^{2+} release in ADO KO cells infected with either control (EV) or ADO-

containing lentivirus, whereas responses to CCh are recovered by ADO re-expression. Mean \pm S.D. n=6-7, *P<0.05, two-way ANOVA with Holm-Sidak post hoc test.

Fig. 5. IL-32 is a target of ADO-catalyzed N-terminal cysteine dioxygenation. (A) Mass spectrometry analyses of the indicated IL-32 N-terminal peptide incubated aerobically with or without recombinant ADO (1h; 37°C), showing a +32 Da shift when incubated with ADO, indicative of the addition of O₂. The small peak at ~845 m/z in the absence of ADO (top panel) was confirmed to correspond to a potassium adduct of the un-oxidized peptide. (B) IL-32, but not asparagine synthetase (ASNS) or JunB, are regulated by hypoxia (1% O₂, 4 h) and ADO in RKO cells. (C) ADO-dependent regulation of IL-32 by hypoxia is observed at the protein but not mRNA level. (D) 293T cells co-transfected with plasmids encoding C-terminally FLAG-tagged IL-32 or an IL-32(C2A) mutant, and either empty pRRL vector (EV), ADO or a catalytically inactive ADO mutant (H112A+H114A), and exposed to hypoxia (1% O₂) for 16 h. IL-32 levels were assessed using an anti-FLAG antibody. Hypoxic accumulation of IL-32 was evident in EV and mutant ADO, but not ADO, co-transfected cells, whilst C2A mutation abolished sensitivity to both hypoxia and ADO overexpression. Note that co-transfection with mutant ADO appears to increase basal levels of IL-32, consistent with possible competition with endogenous ADO for substrate binding.

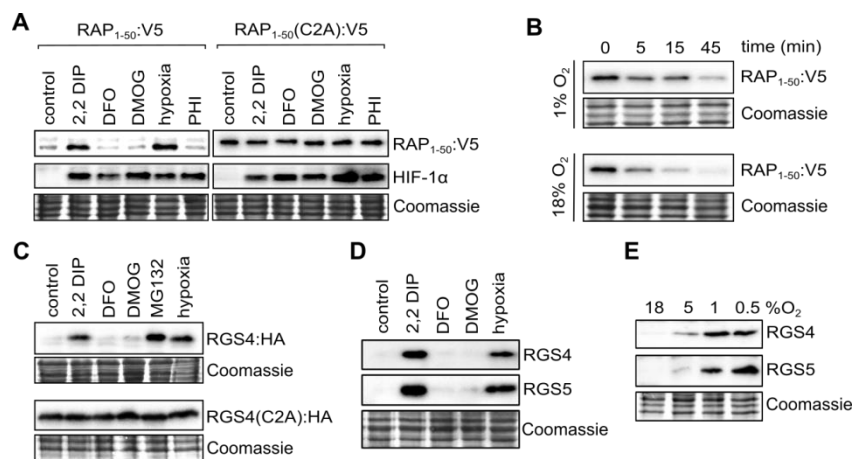


Figure 1

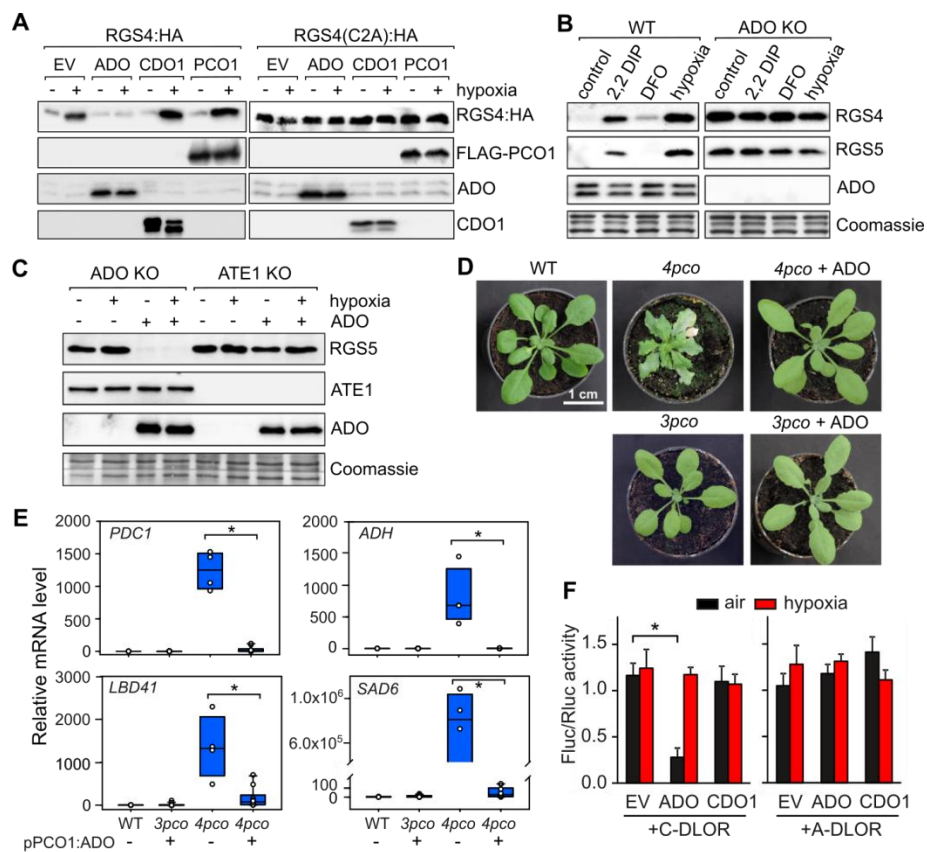


Figure 2

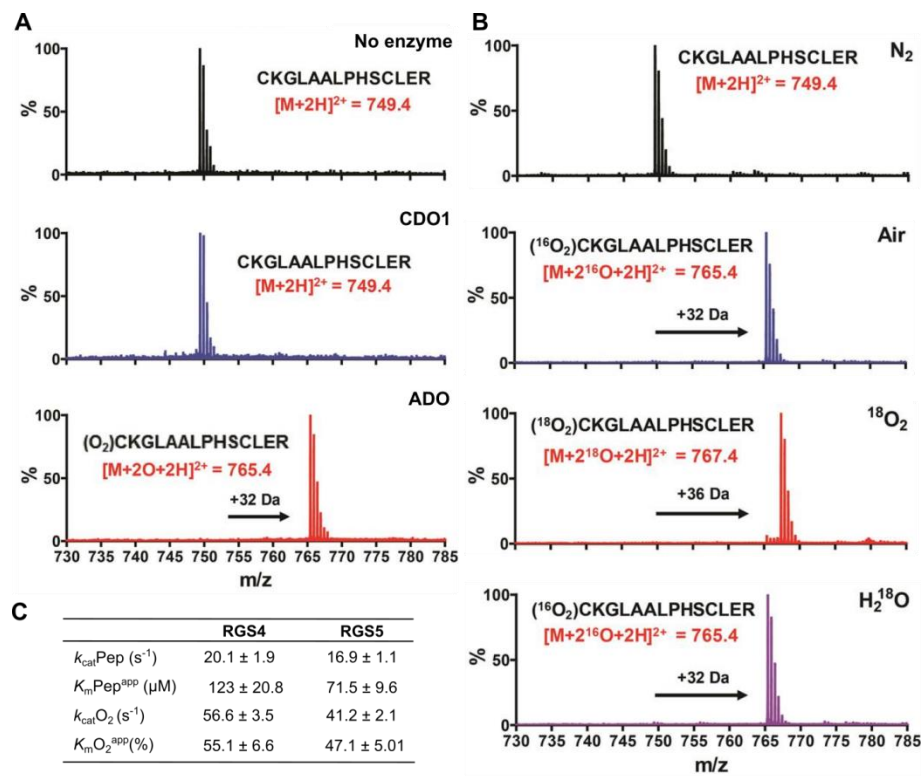


Figure 3

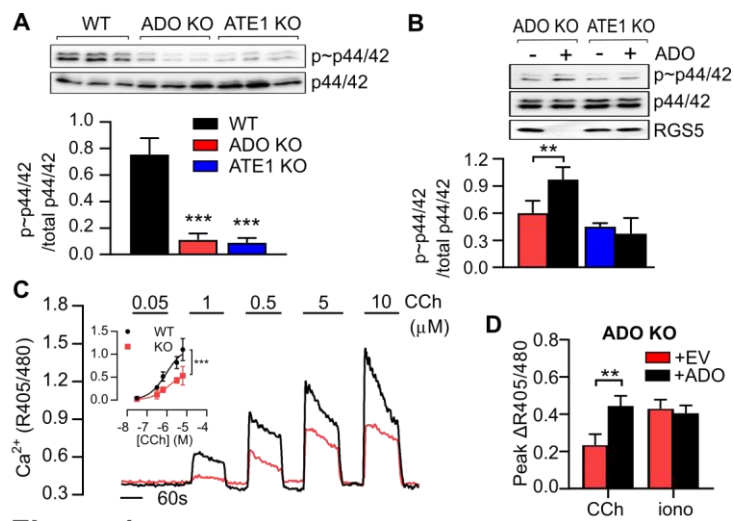


Figure 4

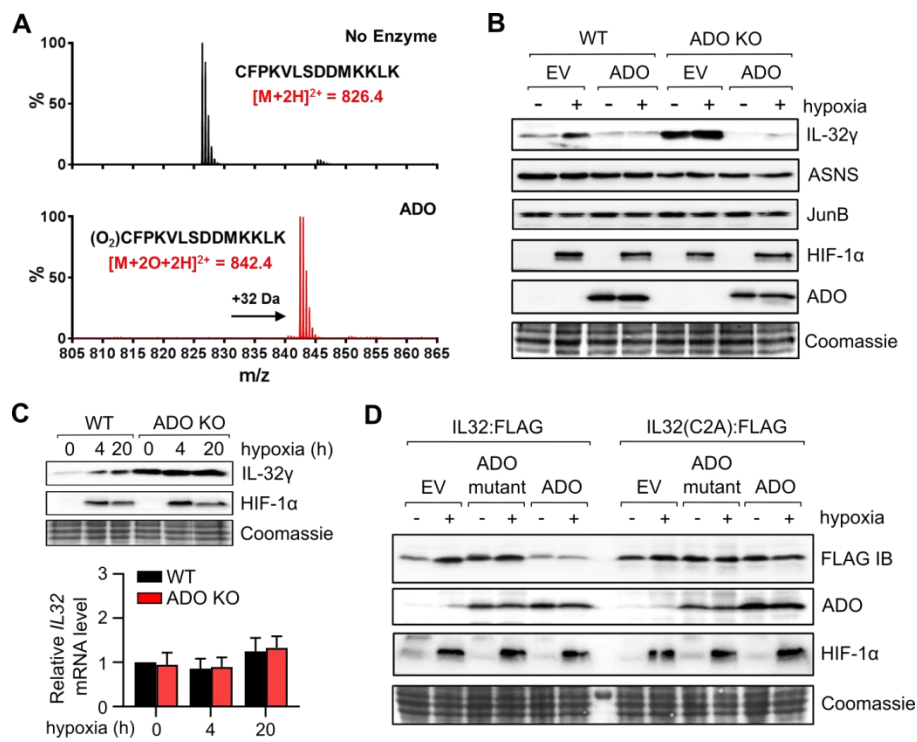


Figure 5



Supplementary Materials for

Conserved N-terminal cysteine dioxygenases transduce responses to hypoxia in animals and plants

Norma Masson^{1,*}, Thomas P. Keeley^{1,*}, Beatrice Giuntoli^{3,4,*}, Mark D. White^{2,*}, Mikel Lavilla Puerta⁴, Pierdomenico Perata⁴, Richard J. Hopkinson², Emily Flashman^{2,a}, Francesco Licausi^{3,4,a},
Peter J. Ratcliffe^{1,5,a**}

*Joint first authors, ^a Joint senior authors, **Corresponding author. Email: peter.ratcliffe@ndm.ox.ac.uk

This PDF file includes:

Materials and Methods

Figure S1 to S18

Reference 29.

Materials and Methods

Reagents

Unless otherwise stated, all reagents were purchased from Sigma-Aldrich. DMOG was from Frontier Scientific. PHI [(1-chloro-4-hydroxy-isoquinoline-3-carbonyl)-amino]-acetic acid was from C.J. Schofield (University of Oxford). MG-132 (Z-Leu-Leu-Leu-CHO) was from BioMol International.

Plasmid Construction

Mammalian expression plasmids.

To generate the RAP₁₋₅₀:GFP:V5 reporter plasmid, a synthetic oligonucleotide (GeneArt, Thermo Fisher Scientific), encoding the first 50 amino acids of the RAP2.12 plant transcription factor (Uniprot Q9SSA8, with either a Cys or Ala at position 2) fused to eGFP was inserted into the pcDNA6.2/V5 DEST Gateway vector. The RGS4₁₋₂₀:GFP reporter plasmid (encoding the first 20 amino acids of the human RGS4 isoform 1, Uniprot P49798-1 fused to eGFP) was produced by ligation of a synthetic oligonucleotide into pcDNA3.1 (GeneArt, Thermo Fisher Scientific). Similarly the RGS4:HA reporter plasmid was produced by ligation of a synthetic cDNA corresponding to full length human RGS4 isoform 1 with a C-terminal HA tag into pcDNA3.1. The RGS4(C2A):HA reporter plasmid was then generated by PCR-based introduction of the Cys2 to Ala mutation. Human ADO cDNA (Image ID 5295674/IRATp970D0689D [BC067740.1]) was from Source BioScience and CDO1 cDNA (pCMV3-Flag-CDO1 [BC024241]) was from Sino Biological. Codon optimized (for mammalian expression) cDNA encoding FLAG-tagged PCO1 (from *A. thaliana*, NCBI reference NM_121516) was produced synthetically (GeneArt, Thermo Fisher Scientific). ADO, CDO1 and FLAG-PCO1 cDNAs were used as templates to produce PCR products which were inserted by BamHI-SnaBI restriction enzyme digest into pRRL-IRES-GFP (provided by K. Kranc, University of London). pRRL-IRES-RFP was then created by replacing the GFP cDNA with RFP (provided by M. E. Cockman, The Francis Crick Institute). Catalytically inactive ADO, in which histidines 112 and 114 were mutated to alanine, was produced as a synthetic oligonucleotide (GeneArt, Thermo Fisher Scientific) and inserted into pRRL-IRES-RFP or GFP as described above. A plasmid encoding human IL-32, tagged with a FLAG epitope at the C-terminal, was from Genscript, and a Cys2 to Ala mutant produced synthetically and ligated into the same vector (pcDNA3+, GeneArt, Thermo Fisher Scientific).

Plant expression plasmids

Synthetic cDNAs codon-optimized for expression in *A. thaliana* (GeneArt, Thermo Fisher Scientific) and encoding human ADO and CDO1 proteins with a C-terminal nuclear localization sequence (PYPGPKVFPPKKRKV) were inserted into pENTR™/D-TOPO™ (Thermo Fisher Scientific). The Gateway® destination vector pH7WG2 for functional Agrobacterium plant transformation was modified to contain the *PCO1* promoter by removing the 35S CaMV promoter (using SpeI and SacI restriction enzymes) and ligating the 1143 bp *PCO1* promoter using Anza T4 DNA ligase (Thermo-Fisher Scientific) to create pH7WG(pPCO1). pENTR-ADO:NLS and pENTR-CDO1:NLS were then recombined into pH7WG(pPCO1) using the LR clonase II enzyme mix (Thermo Fisher Scientific) to generate T-DNA binary plasmids that express either ADO:NLS or CDO1:NLS cDNAs under the control of the PCO1 promoter (pH7WG(pPCO1)ADO/CDO1:NLS). The p2GW7 gateway vector was used for transient transformation of protoplasts to express ADO, CDO1, the bacterial enzyme β -glucuronidase (GUS) or renilla luciferase, under control of the constitutive 35S CaMV promoter (35S:). The 35S:RAP₁₋₂₈ FLuc reporter plasmid expressing firefly luciferase C-terminally fused to the initial 28 amino acids of RAP2.12 has been described(7).

Yeast expression plasmids

The pENTR-ADO:NLS and pENTR-CDO1:NLS plasmids were used for recombination into pAG415GPD-ccdB (provided by Susan Lindquist, Addgene plasmid #14146) to direct the constitutive expression of ADO:NLS and CDO1:NLS in *S. cerevisiae*. The same parent vector pAG415GPD-ccdB was used as a control when expressing the unrelated enzyme β -glucuronidase (GUS). The Cys-containing Dual Luciferase O₂ Reporter (C-DLOR) cDNA and its (Cys to Ala) N-degron pathway insensitive counterpart (A-DLOR) were synthesized (GeneArt, Thermo Fisher Scientific), inserted into pENTR™/D-TOPO™ (Thermo Fisher Scientific) and then recombined into the integrative pAG304GPD-ccdB plasmid (provided by Susan Lindquist, Addgene plasmid # 14136).

Cell culture and hypoxic exposure

U-2OS, RKO, EA.hy926 and HEK 293T cells were cultured in DMEM, and SH-SY5Y in DMEM-F12. C3H/10T1/2 cells were cultured in BME. All media were supplemented with 10% fetal bovine serum, 2mM L-Glutamine, 100 U/ml penicillin and 10 μ g/ml streptomycin, and additionally with endothelial cell growth supplement for EA.hy926 cells. Cells were maintained at 37°C under an atmosphere of 5% CO₂ in air. Hypoxic incubations were conducted within an atmosphere-regulated workstation set at 0.1-5% O₂; 5% CO₂; balance N₂ (Invivo 400, Baker-Ruskin Technologies).

Transient transfection of 293T cells

For transient co-transfection experiments, 293T cells were plated at ~40% confluence and transfected the following day with 1-4 μ g pRRL plasmid and 2 μ g pcDNA3-RGS4:HA using **polyethylenimine reagent**. After 8 h, transfected cells were then split into two separate plates and incubated under normoxia (~18% O₂) or hypoxia (0.1-1% O₂) for 4-16 h. Equal expression of thiol dioxygenase protein was confirmed by a comparison of untagged versus N-terminally FLAG-tagged enzymes. Expression of C-terminally tagged IL-32 and its C2A mutant counterpart was achieved using 1 μ g of the relevant plasmid.

Generation of stable reporter cell lines

To generate stable reporter cell lines, U-2OS or RKO cells at ~40% confluence were transfected with pcDNA6/3 RAP₁₋₅₀:GFP:V5, RGS4₁₋₂₀:GFP or RGS4:HA reporter plasmid using GeneJuice (Novagen). After 24 h, cells were seeded at limiting dilution in selection medium (containing 5-10 μ g/ml Blasticidin S [InvivoGen] for pcDNA6 based reporters) or 0.8-1.5mg/ml G418 [Santa Cruz Biotechnology] for pcDNA3-based reporters) and resistant clones isolated and expanded. Clones stably expressing the reporters were identified by immunoblotting.

Generation of thiol dioxygenase-overexpressing cell lines

To generate ADO, CDO1 and FLAG-PCO1 stable overexpressing lines, cells were incubated with pRRL lentivirus containing supernatant; produced by transfecting 293T cells with the appropriate pRRL vector, together with the lentiviral packaging plasmid, pCMV Δ R8.2 and envelope plasmid, pCMV-VSVG. The 293T viral supernatant was collected 48 h post-transfection, filtered and mixed with 15 μ g/ml Polybrene. The ratio of lentiviral supernatant: cell medium applied to the target cells, was kept between 1:5 and 1:2 to produce >90% infection efficiency (confirmed by GFP fluorescence imaging of the cells). To confirm comparable protein expression of ADO, CDO1 and FLAG-

PCO1enzymes, N-terminally FLAG-tagged versions of ADO and CDO1 were also used to enable the cross-referencing of protein levels by parallel FLAG-immunoblotting.

CRISPR/Cas9-mediated genetic editing of RKO and SH-SY5Y cells

Single guide RNA (sgRNA) design and RNA-ribonucleoprotein (RNP) complex transfections were undertaken with the help of J. Riepsaame (University of Oxford).

Production of sgRNAs

Single guide RNAs (sgRNAs) were transcribed *in vitro* from double-stranded DNA templates. In brief, 60-mer DNA oligos harboring an 18-20-mer protospacer sequence flanked 5' (upstream) by a T7 promoter sequence (TAATACGACTCACTATAGG) and 3' (downstream) by part of the conserved tracrRNA domain sequence (GTTTTAGAGCTAGAAATAGCAA) was annealed to a universal 80-mer oligo (AAAAGCACCGACTCGGTGCCACTTTTTCAAGTTGATAACGGACTAGCCTTATTTTAACTTGCTATTTCTAGCTCTAAAAC) harboring the remainder of the tracrRNA and gap-filled using T4 DNA polymerase (NEB). The resulting double-stranded DNA template was column purified using a DNA Clean & Concentrator kit (Zymo Research) and 500 ng used in a 30µL *in vitro* transcription reaction using the HiScribe T7 High Yield RNA Synthesis Kit, and the manufacturer's protocol (NEB). After 4 h incubation at 37°C, the remaining DNA template was degraded by adding 2 µl of DNaseI and 18 µl water to the reaction. Finally, sgRNAs were purified using a MEGAclean Transcription Clean-Up Kit (Thermo Fisher Scientific) according to the manufacturer's instructions and eluted in 25µL nuclease-free water. Guide RNA concentration and purity was measured using a NanoDrop 1000 spectrophotometer (Thermo Fisher Scientific). For each gene target multiple guide sequences were used to generate the sgRNAs as follows:

CDO1_1: GCGGTACATTGCCCACTCGGTGG

CDO1_2: GGGGCTGGCACGACTCGCTTGGG

ADO_1: GGCGATCCGTTGGATCAAGGAGG

ADO_2: ATGCACATCTACGAGACGGACGG

ATE1_1: GCGTCGGGAACACTCACCGCAGG

ATE1_2: CGTGGACTATTTCCCTAGCGAGG

sgRNAs for CDO1 and ATE1 were designed to span an intron/exon or exon/intron boundary (in order to disrupt splicing), whereas ADO is a single exon gene.

RNP transfection of target cells

Genetically edited cell lines were generated by nucleofection of target cells with a Cas9/sgRNA-RNP complex; produced by combining 1µg of each sgRNA with 5µg HiFi Cas9 Nuclease (IDT) in a total

volume of 2 µl IDT Duplex Buffer (IDT), re-suspending five times and incubating at 37°C for 5 min. Resulting RNP mixes were added directly to cells prior to nucleofection using the Neon Transfection system (Thermo Fisher Scientific), associated Neon Transfection System 10 µL kit (Thermo Fisher Scientific) and recommended nucleofection settings for RKO and SH-SY5Y cell lines. After nucleofection, cells were allowed to recover for 48 h and then seeded at limiting dilutions to grow into individual colonies.

Identification of CRISPR/Cas9 edited clones

Colonies derived from ADO and ATE1 RNP transfections were screened by immunoblot in the first instance to identify candidate edited clones. CDO1 clones together with ADO and ATE1 candidate edited clones (identified by immunoblot) were then further verified by a combination of genomic PCR and Sanger sequencing. Genomic DNA was extracted from cell pellets by incubation in lysis buffer (100mM Tris pH 8.0, 5mM EDTA, 200 mM NaCl, 0.2% SDS and 100 µg/ml Proteinase K) with shaking at 55°C for 2 h, followed by isopropanol precipitation and a 70% ethanol wash. Precipitated genomic DNA was then re-suspended in TE buffer (10mM Tris-HCl pH 8.0 containing 1mM EDTA) by an incubation at 60°C with shaking for 2 h. Genomic target regions were then PCR amplified (CDO1 forward primer: CCACGAGATGGAACAGACCG and reverse primer: GGGGTTAACGATGGCTTGGG; ATE1 forward primer: GCGCCAGGCTTCGCTCTCCAC and reverse primer: CGAGAGTGCCCCCTCCGTCTCG) with Phusion High-Fidelity PCR Master Mix (NEB) according to the manufacturer's protocol using 30 cycles, denaturation at 98°C and an annealing temperature of 63°C. For ADO genomic PCR (ADO forward primer: GCTCAGAGGGGGCTCAAG and reverse primer: GTCTAGCTTGTCATGCAGC), KAPA2G Fast Hotstart Genotyping Mix (Sigma Aldrich) was used as per the manufacturer's protocol using 35 cycles, denaturation at 95°C and an annealing temperature of 64°C. Following analysis of PCR products on agarose gels, DNA was extracted using the QIAquick Gel Extraction Kit (Qiagen) and Sanger sequenced.

Immunoblotting

Cell lysates were prepared as follows: cells (~4 x 10⁶) were washed in phosphate buffered saline and then lysed in 300 µl Igepal lysis buffer (10 mM Tris pH 7.5, 0.25 M NaCl, 0.5% Igepal) containing CompleteTM protease inhibitor cocktail (Sigma Aldrich) at 4°C for 5 min. Samples were centrifuged at 13,000 rpm for 5 min at 4°C, after which the supernatant (cell lysate) was mixed with Laemmli sample buffer. For determination of IL-32 expression by immunoblot, cells were lysed in SDS lysis buffer (50 mM Tris pH 6.8, 2% SDS, 10% Glycerol) and sonicated, before mixing with Laemmli sample buffer. Proteins were separated by SDS-polyacrylamide gel electrophoresis, transferred to polyvinylidene difluoride membrane (Immobilon-P, Millipore) and blocked in either 4% fat free milk (in phosphate-buffered saline containing 0.1% Tween 20) or 2% bovine serum albumin (in Tris-buffered saline containing 0.1% Tween 20) for p44/42 MAPK immunoblotting. Primary antibodies used were: V5 (MCA1360, Serotec), GFP (11814460001, Sigma Aldrich), HIF-1α (610959, BD Biosciences), HRP conjugated HA (3F10, Sigma Aldrich), HRP-conjugated FLAG (A8592, Sigma-Aldrich), ADO (ab134102, Abcam), ATE1 (HPA038444) and CDO1 (HPA057503) from Atlas Antibodies. Phospho-p44/42 MAPK (Thr202/Tyr204) antibody (9101), p44/42 MAPK Antibody (9102), RGS4 (15129) and JunB (3753) from Cell Signaling Technologies, RGS5 (sc-514184), IL-32 (sc-517408) and ASNS (sc-365809) from Santa Cruz Biotechnology. HRP-conjugated secondary antibodies (DAKO) and chemiluminescence substrate (West Dura, 34076, Thermo Fisher Scientific) were used to visualize proteins, using a ChemiDoc XRS+ imaging system (BioRad). After immunoblot analysis, membranes were

stained with Coomassie brilliant blue to visualize separated proteins, and this was used as a reference of sample loading. Densitometric analysis was performed using ImageJ software (NIH) and values presented relative to Coomassie blue staining. For analysis of p44/42 MAPK phosphorylation, phospho- and total-p44/42 MAPK were probed on separate blots and corrected for their respective Coomassie stain. Loading-corrected phospho-p44/42 MAPK signal was then expressed as a ratio to the corresponding total p44/42 MAPK signal.

Real-time quantitative PCR

Mammalian cells were lysed in TRIzol and mRNA extracted by phase separation. Equal amounts of mRNA were used for cDNA synthesis using the High Capacity cDNA Kit (Applied Biosystems). Expression analyses were performed using Fast SYBR Green Master Mix on a StepOne thermocycler (both from Applied Biosystems, now Thermo Fisher Scientific) using the $\Delta\Delta C_t$ method. Primers used for analysis were as follows: RAP₁₋₅₀:GFP:V5 reporter transcript (forward primer: ACCCCGACCATATGAAGCAG and reverse primer: GGCCCTGGTCTTGTAAGTTGC), HPRT (forward primer: GACCAGTCAACAGGGGACAT and reverse primer: AACACTTCGTGGGGTCCTTTTC), RGS4 (forward primer: GCAAAGGGCTTGCAGGTCT and reverse primer: CAGCAGGAAACCTAGCCGAT), RGS5 (forward primer: TGGTGACCTTGTCATTCCG and reverse primer: TTGTTCTGCAGGAGTTTGTC), and IL32 (forward primer: CTTCCCGAAGGTCCTCTCTGAT and reverse primer: GTCCTCAGTGTCACACGCT). Primers used for analysis of mouse transcripts were as follows: Hprt (forward primer: GTTGGATACAGGCCAGACTTT and reverse primer: CCACAGGACTAGAACACCTGC) and Rgs4 (forward primer: TGCCTTTCTCTCCTCGCTAA and reverse primer: CAGCCGATGTTTCATGTCCT).

Intracellular Ca²⁺ measurements

SH-SY5Y parental (WT) and ADO (CRISPR/Cas9) edited cells (KO), seeded on coverslips the previous day, were loaded with 5 μ M Indo-1AM (Life Technologies) a UV light-excitable, ratiometric Ca²⁺ indicator for 60 min at room temperature. Coverslips were then mounted in a continuous perfusion system above a microspectrofluorimeter (Nikon Diaphot 200) equipped with a xenon lamp light source and photomultiplier tubes (Thorn EMI). Indo-1 was excited at 340 nm and emitted fluorescence intensity measured at 405 nm and 495 nm. The ratio of fluorescence emission (R405/495) was used as a measure of intracellular Ca²⁺. Coverslips were perfused with bicarbonate-buffered Tyrode solution (117 mM NaCl, 4.5 mM KCl, 1 mM CaCl₂, 1 mM MgCl₂, 2.5 mM NaHCO₃, 11 mM Glucose) at 37°C and gassed with 5% CO₂ in air. Carbachol (CCh, 0.05 to 10 μ M) or ionomycin (Iono, 0.1 μ M) were prepared as separate solutions and administered via a rapid, in-line switching mechanism. To account for variation in drug stability or dye loading, the WT and ADO KO cells were tested alternatively. Raw fluorescence intensity values were background-corrected and smoothed using Prism 7 (GraphPad). Peak change above baseline was measured by using an ‘analyze peaks’ algorithm, plotted against [CCh] and subjected to 3 parameter log(agonist) vs response non-linear regression analysis.

Plant assays

A. thaliana growth conditions

A. thaliana Columbia-0 (Col-0) was used as the wild-type ecotype. Seeds were sown in moist soil containing pit and perlite in a 3:1 ratio, stratified at 4°C in the dark for 48 h and then germinated at

22°C day/18°C night with a photoperiod of 12 h of light and 12 h of darkness with $100 \pm 20 \mu\text{mol photons m}^{-2} \text{ s}^{-1}$ intensity. Adult plants at the vegetative stage (i.e. 7 weeks of age in the case of *4pco* and *4pco+CDO1* plants and 4 weeks for the remaining genotypes) were used for the analyses. Seeds for *4pco* and *4pco+CDO1* plants were sown 3 weeks earlier than the other genotypes to enable the parallel harvest of plants.

4pco mutant generation

The quadruple *4pco* mutant was generated by subsequent rounds of crossing by manual pollination of Arabidopsis T-DNA mutants followed by PCR-assisted selection of homozygous insertions in the relevant genes. All T-DNA mutant lines were purchased from the Nottingham Arabidopsis Stock Centre (uNASc). T-DNA insertion line for *PCO1* (*At5g15120*) was N451210, for *PCO2* (*At5g39890*) was N116554, for *PCO4* (*At2g42670*) was N471015 and for *PCO5* (*At3g58670*) was N684949. The allelic status of each T-DNA insertion was tested by two parallel genomic PCR reactions using the following primer sets: insPCO1fw (AATGGTGGTCCTGGTGTTATTC) with insPCO1rv (GCAAGGTAACAACGACAAACAA) and insPCO1fw with LB1GK (ATATTGACCATCATACTCATTGC) for *PCO1*, insPCO2fw (TGTTCTTTTGCCCTCTTCTCTC) with insPCO2rv (TCCGGGTGATGTACAAATACAA) and insPCO2rv with dspm5 (CGGGATCCGACACTCTTTAATTAAGTACTGACTC) for *PCO2*, insPCO4fw (CATGAGCCTGAAGTCTGCAAAA) with insPCO4rv (GCCGTCATCTCAGTATCCTTCA) and insPCO4fw with LB1GK for *PCO4*, insPCO5fw (GCCCATTTAGGTAGCTGCAGTG) with insPCO5rv (AGCTTCCTGTTTCGAGACCAA) and insPCO5fw with LBb1 (GCGTGGACCGCTTGCTGCAACT) for *PCO5*.

A. thaliana transformation and genotyping of human ADO and CDO1 expressing plants

Quadruple *4pco* mutant plants were transformed by Agrobacterium-mediated infiltration using the floral dip method to enable expression of human ADO or CDO1 with a C-terminal nuclear localization sequence under the control of the *PCO1* promoter (*pPCO1:ADO:NLS* or *pPCO1:CDO1:NLS*). Briefly, *PCO1*^{-/-}; *PCO2*^{-/-}; *PCO4*^{-/-}; *PCO5*^{+/-} (T₀) plants were used for T-DNA insertion. The allelic status of the *PCO5* locus in the T₂ population was then assessed by two parallel genomic PCR reactions employing insPCO5fw and LBb1 (T-DNA specific) reverse primer, or insPCO5fw and insPCO5rv primers. The presence of the transgene was evaluated by resistance to hygromycin and confirmed by PCR (attB1 forward primer: GGGACAAGTTTGTACAAAAAAGCAGGCT and either ADO reverse primer: AGCAGGTCCTTCAACAGCGT or CDO1 reverse primer: CGAAAGCGTGGCAGGTATCG).

A. thaliana gene expression analyses

A T₂ segregating population was used for the phenotypic and molecular characterization of the ADO or CDO1 effect, after genotyping for T-DNA insertion in the *PCO5* locus as described above. RNA was extracted from fully developed rosette leaves as follows: following lysis in a buffer composed of 50 mM TrisHCl pH 8, 300 mM NaCl, 5mM EDTA pH 8, 2% SDS and 180 mM β-mercaptoethanol, cell debris was precipitated in the presence of 400 mM KCl and mRNA isolated from the supernatant by phase separation and ethanol precipitation. Equal mRNA amounts were processed into cDNA with the Maxima First Strand cDNA Synthesis Kit (Thermo Fisher Scientific). Real-time qPCR amplification was carried out in the ABI Prism 7300 sequence detection system (Applied Biosystems), using the PowerUp™ SYBR® Green Master Mix (Thermo Fisher Scientific) and 15 ng cDNA in each reaction. Primers used for analysis of transcript levels from the following genes were *PYRUVATE DECARBOXYLASE 1* (*At4g33070*) (*PDC1* forward primer: CACAGAATCTTCAATGTTCTTACC and reverse primer: CCATGATAAAGCGTACATGGAA), *ALCOHOL DEHYDROGENASE* (*At1g77120*), (*ADH* forward primer:

TATTCGATGCAAAGCTGCTGTG and reverse primer: CGAACTTCGTGTTTCTGCGGT), *LATERAL ORGAN BOUNDARY DOMAIN CONTAINING PROTEIN 41* (*At3g02550*) (*LBD41* forward primer: TGAAGCGCAAGCTAACGCA and reverse primer: ATCCCAGGACGAAGGTGATTG), *STEAROYL-ACYL CARRIER PROTEIN Δ9-DESATURASE6* (*At1g43800*) (*SAD6* forward primer: TTGGCAACCCGCTTCTTTCTTACC and reverse primer: TTTCCCTCAGCTCACGAACCTG), *ACT2* (*At3g18780*) (*ACT2* forward primer: GGCAAGTCATCACGATTGG and reverse primer: CAGCTTCCATTCCCACAAAC), *At2g28390* (forward primer: AACTCTATGCAGCATTTGATCCACT and reverse primer: TGATTGCATATCTTTATCGCCATC) and as reference gene *Ubiquitin10* (*At4g05320*) (*UBQ10* forward primer: GGCCTTGTATAATCCCTGATGAATAAG and reverse primer: AAAGAGATAACAGGAACGGAAACATAGT). Relative gene expression values were calculated with the $\Delta\Delta C_t$ method.

A. thaliana protoplast assays

Protoplasts were isolated from wild type leaves, following an enzymatic digestion in an isotonic solution containing 0.4 M mannitol, 20 mM KCl, 20 mM MES (pH 5.7), 10 mM CaCl₂, 1% cellulase (w/v), and 0.4% macerozyme (w/v). Cells were washed in 154 mM NaCl, 125 mM CaCl₂, 5 mM KCl and 2 mM MES (W5 solution), and re-suspended up to 5×10^5 cells ml⁻¹ in 0.4 M mannitol, 15 mM MgCl₂, 5 mM MES. Protoplasts (100 μ l) were transformed with naked DNA using an equal volume of a 40% PEG 4000 (w/v), 100 mM CaCl₂ and 200 mM mannitol solution. Transfections of RAP₁₋₂₈-Fluc reporter construct with either human ADO, CDO1 or control GUS, were carried out in biological quintuplicate, using 2.5 μ g of reporter construct in each and variable amounts of the effector constructs, as specified in the text. An equal amount of a *35S:Rluc* construct expressing renilla luciferase was included in every transfection, to permit the normalization of the firefly luciferase signal. W5 was used to block the transfection and cells were incubated in 500 mM mannitol, 4 mM MES, and 20 mM KCl. The stability of the RAP₁₋₂₈-Fluc protein was evaluated by means of the Dual Luciferase Assay kit (Promega), following the manufacturer's protocol. 18 h after transfection protoplasts were spun down from the suspension, flash frozen in liquid nitrogen and lysed in 50 μ l Passive Lysis Buffer. Six μ l cleared lysate was then used for the measurements. Relative luciferase activity was expressed as Fluc/Rluc.

Yeast assays

Yeast transformation

The *S. cerevisiae* strain MAV203 was transformed with plasmids using the LiAc method to result in expression of DLOR, ADO and CDO1. The parental (unrecombined) plasmid or plasmid expressing GUS was used as negative control. Transformed colonies were selected based on auxotrophy complementation and the expression of ADO, CDO1 and control β -glucuronidase (GUS) assessed by real-time quantitative PCR (ADO forward primer: CGGTGGTGGACAAAGGCCTA, ADO reverse primer: AGCAGGTCCTTCAACAGCGT, CDO1 forward primer: CTCTTTTCGCTTGGCCGGAC, CDO1 reverse primer: CGAAAGCGTGGCAGGTATCG, GUS forward primer: CTCTGGCAACCGGGTGAAGG, GUS reverse primer: CCTTCACTGCCACTGACCGG), using the *Actin1* housekeeping gene as the reference (ACT1 forward primer: CCATCCAAGCCGTTTTGTCC, ACT1 reverse primer: GGCGTGAGGTAGAGAGAAACC). The selected colonies were grown on liquid synthetic drop-out medium overnight. Subsequently, the cultures were diluted to OD₆₀₀ 0.1 and treated for 6 h under either aerobic (21% O₂) or hypoxic (1% O₂) conditions. At the end of the treatments, cells were collected by centrifugation and used for protein immunoblotting and luciferase activity assays.

Immunoblotting of yeast proteins

Total protein was extracted in a buffer containing 50 mM Tris-HCl pH 7.6, 1 mM EDTA, 100 mM NaCl, 2% SDS and 0.05% Tween-20, separated by SDS-PAGE on 10% acrylamide midgels (Bio-Rad) before transfer onto a polyvinylidene difluoride membrane (Bio-Rad). A polyclonal anti-PpLuc (G7451 Promega) and a monoclonal anti-RrLuc (MAB4410, Millipore) were used at 1:1,000 dilutions to detect firefly and renilla luciferases, respectively. Protein loading was evaluated by Coomassie staining of the membrane.

Yeast Luciferase assay

Yeast extracts were prepared and luciferase activity assayed using the Dual Luciferase Reporter Assay kit (Promega) and the manufacturer's protocol. Luciferase measurements were taken using a Lumat 9507 luminometer (Bechtold).

Recombinant enzyme assays

Recombinant human ADO and CDO1 protein production

Synthetic cDNAs codon-optimized for expression in *E. coli* and encoding human ADO and CDO1 (GenScript) were used as templates to generate PCR products which were inserted into the NdeI and XhoI restriction sites of pET28a. The resulting plasmid was transformed into Rosetta (DE3) competent *E. coli* cells (Merck) for recombinant N-terminal His-tagged protein production in 2YT media supplemented with 40 $\mu\text{g mL}^{-1}$ kanamycin. Cultures were grown to an OD₆₀₀ of approximately 0.8 by shaking at 180 rpm and 37°C, before being induced with 0.5 mM IPTG overnight at 20°C. Cells were harvested by centrifugation at 10000g for 10 min. Cell pellets were then re-suspended in 50 mM Tris, 400 mM NaCl pH 7.5, supplemented with DNase I (Thermo Fisher Scientific) and a Complete™ EDTA-free protease inhibitor cocktail (Sigma Aldrich) before being lysed by sonication. Cellular debris was removed by centrifugation at 48000g for 30 min and filtration through a 0.45 μm membrane. The soluble supernatant was loaded onto an equilibrated HisTrap HP column (GE Healthcare, now Sigma Aldrich) and washed with resuspension buffer containing increasing concentrations of imidazole until a definitive A_{280 nm} peak was collected. Imidazole was then removed using a desalting column. Protein purity was verified by SDS-PAGE and protein concentrations were estimated using A_{280 nm} measurements.

Activity assays using recombinant human ADO and CDO1 protein

The enzymatic activities of recombinant His-tagged human ADO and CDO1 proteins were examined by incubating 400 μM synthesized peptide (GL Biochem) corresponding to the first 14 amino acids of the Met-excised N-terminus of RGS4 and RGS5 (i.e. RGS4₂₋₁₅ and RGS5₂₋₁₅, respectively) with and without 4 μM enzyme in a bench top thermomixer at 37°C for 1 h. The following reaction buffer was used: 5 mM Tris (2-carboxyethyl)phosphine hydrochloride (TCEP), 20 μM FeSO₄ and 1 mM ascorbate were added to buffer (50 mM Bis-Tris Propane, 50 mM NaCl, pH 7.5) to maintain a reductive environment and provide exogenous cofactors. The reaction was quenched by mixing the sample 1:1 with 1% formic acid (v/v). Oxidation was monitored by ultrahigh-performance liquid chromatography (UPLC) mass spectrometry (MS) using an Acquity UPLC system coupled to a Xevo G2-S Q-ToF mass spectrometer (Waters) operated in positive electrospray mode. Instrument parameters, data acquisition, and data processing were controlled by MassLynx 4.1 with source conditions adjusted to maximize sensitivity and minimize fragmentation. Samples were injected onto a Chromolith Performance RP-18e 100 2-mm column (Merck) heated to 40°C and eluted at 0.3 ml/min using a gradient of 95% deionized water supplemented with 0.1% (v/v) formic acid to 95%

acetonitrile. The same experimental conditions were used to examine the activity of His-tagged human ADO with a peptide (Genscript) corresponding to the first 14 amino acids of the Met-excised N-terminus of IL-32 (i.e. IL-32₂₋₁₅).

Tandem mass spectrometric analysis of RGS and IL-32 peptides

Fragmentation spectra of the RGS4₂₋₁₅, RGS5₂₋₁₅ substrate and (recombinant enzyme reaction) product ion species were obtained to verify the position of the modification using a NanoAcquity-UPLC coupled to an Orbitrap Elite mass spectrometer possessing an EASY-Spray nano-electrospray ion source (Thermo Fisher Scientific). The peptides were trapped on an in-house packed guard column (75 μ m i.d. x 20 mm, Acclaim PepMap C18, 3 μ m, 100 Å) using solvent A (0.1% formic acid in water) at a pressure of 140 bar and separated on an EASY-spray Acclaim PepMap® analytical column (75 μ m i.d. x 50 mm, RSLC C18, 3 μ m, 100 Å) using a linear gradient (length: 100 min, 3% to 60% solvent B (0.1% formic acid in acetonitrile), flow rate: 300 nL/min). The separated peptides were electrosprayed directly into the mass spectrometer that was operating in a data-dependent mode using a collision-induced dissociation (CID) based method. Full scan MS spectra (scan range 350-1500 m/z, resolution 120000, AGC target 1e6, maximum injection time 250 ms) and subsequent CID MS/MS spectra (AGC target 5e4, maximum injection time 100 ms) of the 10 most intense peaks were acquired in the Ion Trap. CID fragmentation was performed at 35% of normalized collision energy and the signal intensity threshold was kept at 500 counts. The CID method used performs beam-type CID fragmentation of the peptides. The most abundant precursor charge states were subjected to electron-transfer dissociation (ETD) fragmentation. Ion peaks were analyzed using PEAKS Studio 8.5 (Bioinformatics Solutions Inc.).

Fragmentation spectra of IL-32₂₋₁₅ substrate and product peptide ions were obtained using a targeted approach on the UPLC-MS described above, selecting the $[M+2H+]^{2+}$ parent species for CID with a typical energy ramp of 30 to 40 eV. Analysis was carried out with the same source settings, flow rate and column elution conditions described above for initial activity assays. Daughter ions were manually assigned by examining the spectra in MassLynx 4.1.

Determining the source of O-atoms used during recombinant human ADO catalyzed modification of RGS peptides

The source of oxygen atoms used to modify RGS peptides during reaction with purified recombinant His-tagged human ADO was verified by monitoring the mass shifts in the product peptides following incubation with N₂, air (i.e. ¹⁶O₂), ¹⁸O₂ and H₂¹⁸O. 100 μ L of 400 μ M RGS4₂₋₁₅ or RGS5₂₋₁₅ dissolved in reaction buffer (described above), was rendered anaerobic in a septum sealed glass vial by purging the sample with 100% N₂ for 10 min at 100 mL min⁻¹ using a mass flow controller (Brooks Instruments). 4 μ M ADO was added to the solution using a gas-tight Hamilton syringe and the reaction mixture was purged with a balloon containing approximately 0.7 L N₂, air (i.e. ¹⁶O₂) or ¹⁸O₂ for 10 min at room temperature. The samples were then transferred to a water bath for an additional 20 min incubation at 37°C, before being quenched 1:1 with 1% formic acid (v/v) and analysed by UPLC-MS, as described above. Reactions in the presence of H₂¹⁸O were conducted as described for the air sample, replacing 75% of the water used in the final reaction sample with H₂¹⁸O.

Kinetic analysis of recombinant human ADO with RGS and IL-32 peptides under atmospheric conditions

The kinetic parameters of purified recombinant His-tagged human ADO under atmospheric conditions were determined by measuring the rate of RGS peptide oxidation at different substrate concentrations using a stopped assay. Reaction mixtures (buffer as above) containing 15 to 1000 μ M RGS4₂₋₁₅ or RGS5₂₋₁₅, or IL-32₂₋₁₅ were mixed with 0.05 to 0.2 μ M human ADO and incubated at 37 °C before being quenched at regular time intervals 1:10 with 1% formic acid (v/v). Oxidation was monitored by

high throughput MS using a RapidFire RF360 sampling robot connected to an Agilent 6530 Accurate-Mass Q-ToF mass spectrometer (Agilent) operated in positive ion mode. Source conditions were adjusted to maximize sensitivity and minimize fragmentation. Samples were injected onto a C-4 solid phase extraction (SPE) cartridge equilibrated with deionized water containing 0.1% formic acid (v/v), washed with the equilibration solution and eluted in 85% acetonitrile and 0.1% formic acid (v/v). Turnover was quantified by comparing the integrated area underneath the product and substrate ions extracted from the total ion current chromatogram using the RapidFire Integrator software. All figures and kinetic parameters were generated using Prism (GraphPad).

Determining the O₂ sensitivity of recombinant human ADO

The kinetic parameters of purified recombinant His-tagged human ADO with molecular oxygen were determined by measuring the rate of RGS peptide turnover at different O₂ concentrations using a stopped assay. A concentration of peptide that generated the highest level of activity under atmospheric conditions was used for analysis (i.e. 320 μ M). 100 μ L aliquots of RGS4₂₋₁₅ or RGS5₂₋₁₅ were prepared in reaction buffer (described above), transferred into a septum sealed glass vial, and equilibrated with different ratios of nitrogen and oxygen gas (0 to 80% O₂) for 10 min using a mass flow controller (Brooks Instruments). 1 μ L of 0.1 μ M recombinant human ADO was added to the solution using a gas-tight syringe (Hamilton) to initiate the reaction, which was allowed to proceed for 1 min (i.e. within the linear range of activity). Turnover was terminated by injecting 10 μ L 10% formic acid and oxidation was analyzed by high throughput MS, as above.

Activity assays using recombinant human ADO and additional N-Cys peptides

Peptides (Genscript and GL Biochem) representing the N-terminus of candidate ADO substrates were synthesized as N-terminal amine 14-mers and incubated with recombinant ADO under aerobic conditions at 37°C in reaction buffer using a peptide: enzyme ratio of 100 μ M: 0.1 μ M. Reactions were quenched with 1% formic acid (v/v) at 0 and 1 minute time points and ADO activity measured using UPLC-MS as described above. Turnover was quantified by comparing the integrated area underneath the product and substrate ions extracted from the total ion current chromatogram using MassLynx 4.1, enabling determination of specific activity.

ADO competition assays with cysteine and cysteamine

The influence of free cysteine and cysteamine on ADO turnover was determined by monitoring the activity of 0.2 μ M recombinant ADO with 320 μ M RGS5₂₋₁₅ in the presence of 5 μ M to 500 mM cysteine or cysteamine. Single time points were taken in triplicate by quenching the reaction with 1% formic acid (v/v) after 30 seconds. The level of turnover was analyzed by high throughput MS, as described above, and normalized to activity measurements in the absence of cysteine or cysteamine. IC₅₀ values were estimated using the log inhibitor versus normalized response model in Prism.

Phylogenetic analysis of ADO/PCO domain-containing proteins

The Pfam database (EMBL-EBI) was used to collate protein sequences with sufficient similarity to a ADO/PCO conserved sequence, predefined by comparison of 21 seed (known) ADO/PCO1 proteins (PF07847). Evolutionary history between these sequences was then inferred by the Maximum Likelihood method using MEGA X.

Statistical analyses

Mammalian cells

Reference to an experiment denotes a set of samples collected on a single day, whereas an independent clone denotes separate cultures propagated from a single parent culture. All immunoblots shown are representative of at least three experiments or independent clones. Where quantified, data represent the mean \pm S.D. Statistical significance was tested by either a two-sided, one-way (Fig. 4A) or two-way (4B and D, S8) ANOVA with Holm-Sidak post hoc test. Statistical analysis relevant to a specific data set is described in detail within the appropriate section. Transcript analyses are representative of three independent experiments and are expressed as mean \pm S.D.

Arabidopsis thaliana

A segregating T₂ population (n=68) from the initial transformation of *pPCO1:ADO* into a quadruple *pco* mutant genotype (*pco1/2/4/5^{+/-}*) was used for initial gene expression analysis. Four genotypic classes were examined: wild type (n=5), *4pco* (n=4), *3pco+ADO* (n=17), *4pco+ADO* (n=10). The statistical significance of the effect of ADO overexpression on gene expression in *Arabidopsis* was assessed by non-parametric one-way ANOVA on ranks, followed by a Mann-Whitney Rank Sum Test comparing *3pco+ADO* and *4pco+ADO* (Figure 2G and fig. S10A). In additional analyses, an independent *pPCO1:ADO* line from the one shown in Figure 2F (i.e. line #2) was derived from the quadruple *pco* mutant genotype (*pco1/2/4/5^{+/-}*) and compared with a similarly derived *pPCO1:CDO1* line (fig. S10B and C). From the above T₂ segregating population for *pPCO1:ADO*, *pPCO1:ADO* expressing plants in the triple mutant genotype (*pco1/2/4/5^{+/+}*) were also analyzed as an additional control. In these additional experiments (fig. S10B and C) the following genotypic classes were examined: wild type (n=5), *4pco* (n=5), *3pco+ADO* (n= 5), *4pco+ADO*, (n=5) *4pco+CDO1* (n=5).

S. cerevisiae

Relative luciferase activity data (Figure 2H) represent the mean \pm S.D of 5 independent clones. Statistical significance was tested by two-way ANOVA and a Holm-Sidak multiple comparison test. Yeast immunoblots are representative images following analysis of two independent clones of each genotype and were in parallel with luciferase activity data (fig. S11B).

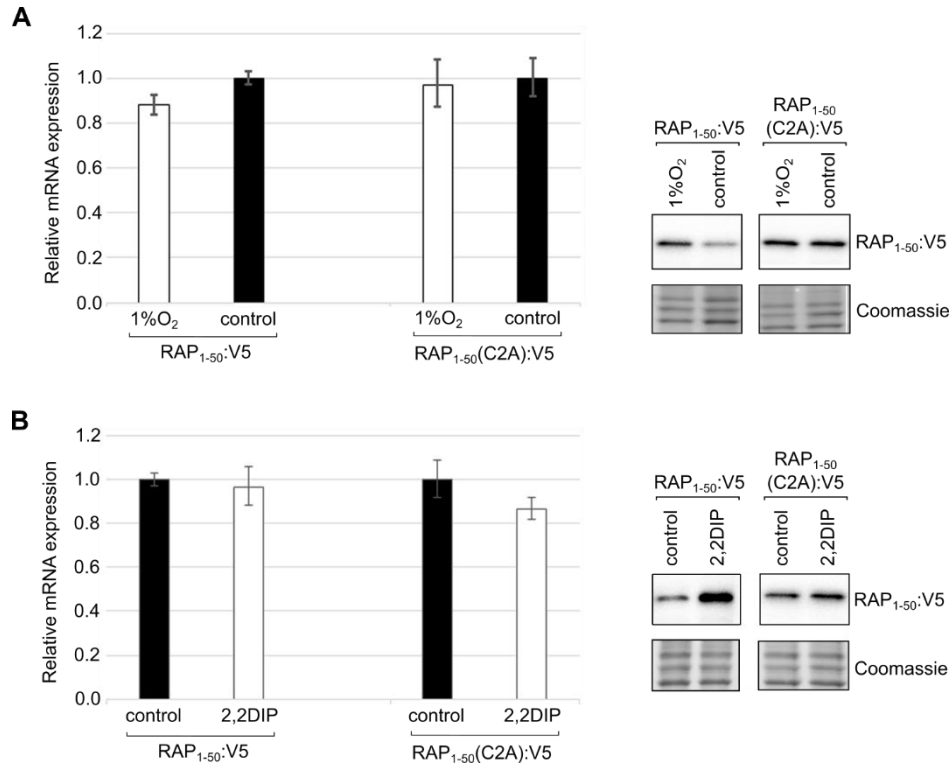


Figure S1. Comparison of changes in RAP₁₋₅₀:GFP:V5 reporter protein and transcript level in cells exposed to hypoxia or dipyrindyl.

U-2OS cells stably expressing a wild-type RAP₁₋₅₀:GFP:V5 reporter (RAP₁₋₅₀:V5) or its C2A mutant (RAP₁₋₅₀ (C2A):V5) were exposed to (A) hypoxia (1% O₂) or (B) dipyrindyl (2,2DIP, 100μM) for 4 h. The effect of the treatments on reporter transcript levels are shown as mean ± SD n=4, alongside representative protein immunoblots from cells harvested in parallel. RAP₁₋₅₀:GFP-V5 transcript level is unaffected by exposure to hypoxia or dipyrindyl, while RAP₁₋₅₀:GFP:V5 protein level is increased.

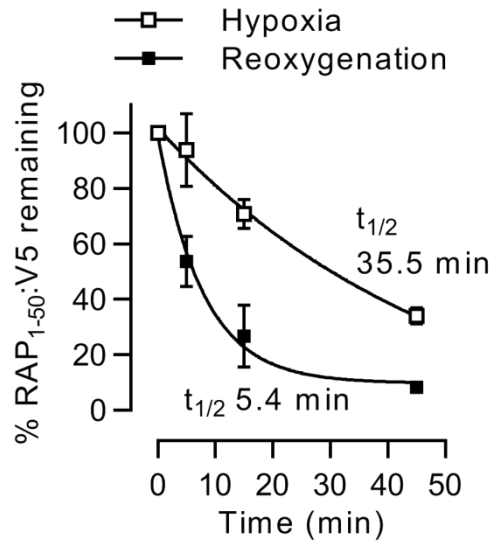


Figure S2. Quantification of RAP2.12 fusion protein half-life under hypoxic and reoxygenated conditions.

U-2OS cells stably expressing a wild-type RAP₁₋₅₀:GFP:V5 reporter (RAP₁₋₅₀:V5) were exposed to hypoxia (1% O₂) for 16 h, then treated with cycloheximide (100μM, 10min), then maintained in hypoxia or re-oxygenated for the indicated times. Densitometric analysis of blots shown in Fig. 1B, and two further independent experiments were conducted, plotted against time and subjected to exponential decay regression analysis to determine a half-life ($t_{1/2}$), as indicated on the graph.

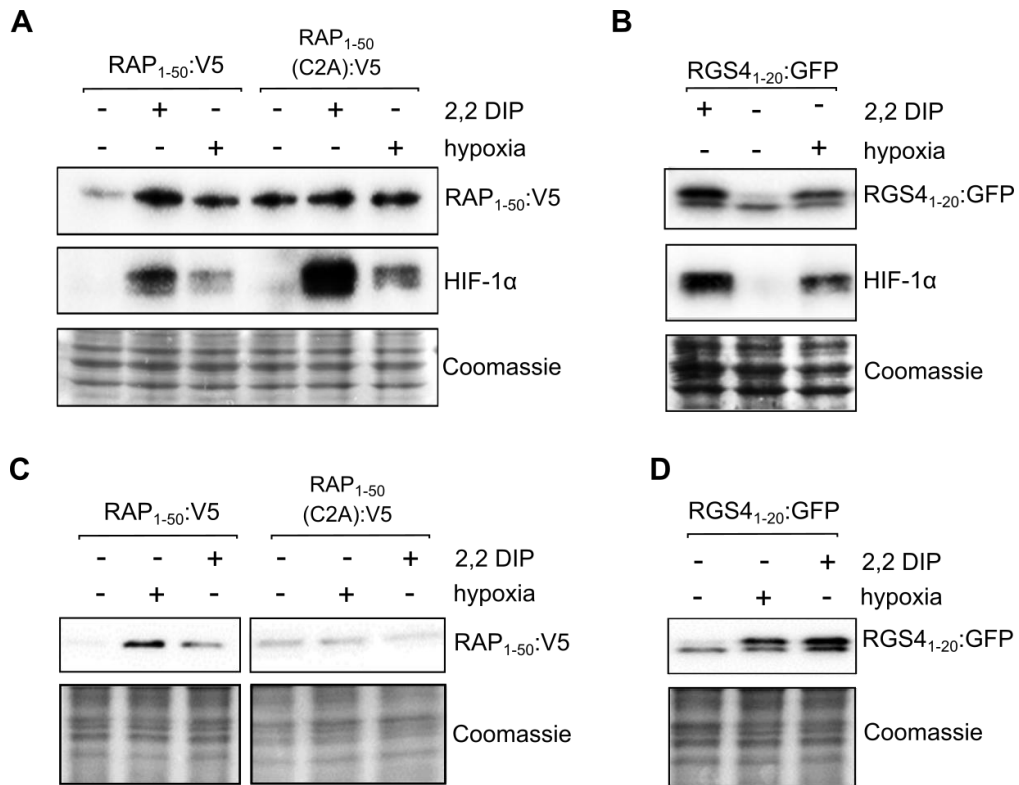


Figure S3. Concordant regulation of plant RAP2.12 and animal RGS4 fusion protein reporters in different human cells.

U-2OS cells (A and B) or RKO cells (C and D) stably expressing either the wild type or C2A mutant RAP₁₋₅₀:GFP:V5 reporters (RAP₁₋₅₀:V5, A and C) or wild-type RGS4₁₋₂₀:GFP (B and D) fusion proteins. Immunoblots show fusion protein levels in cells exposed to hypoxia (1% O₂) or dipyridyl (2,2DIP, 100μM) for 4 h. In A and B, HIF-1α immunoblots are shown for comparison.

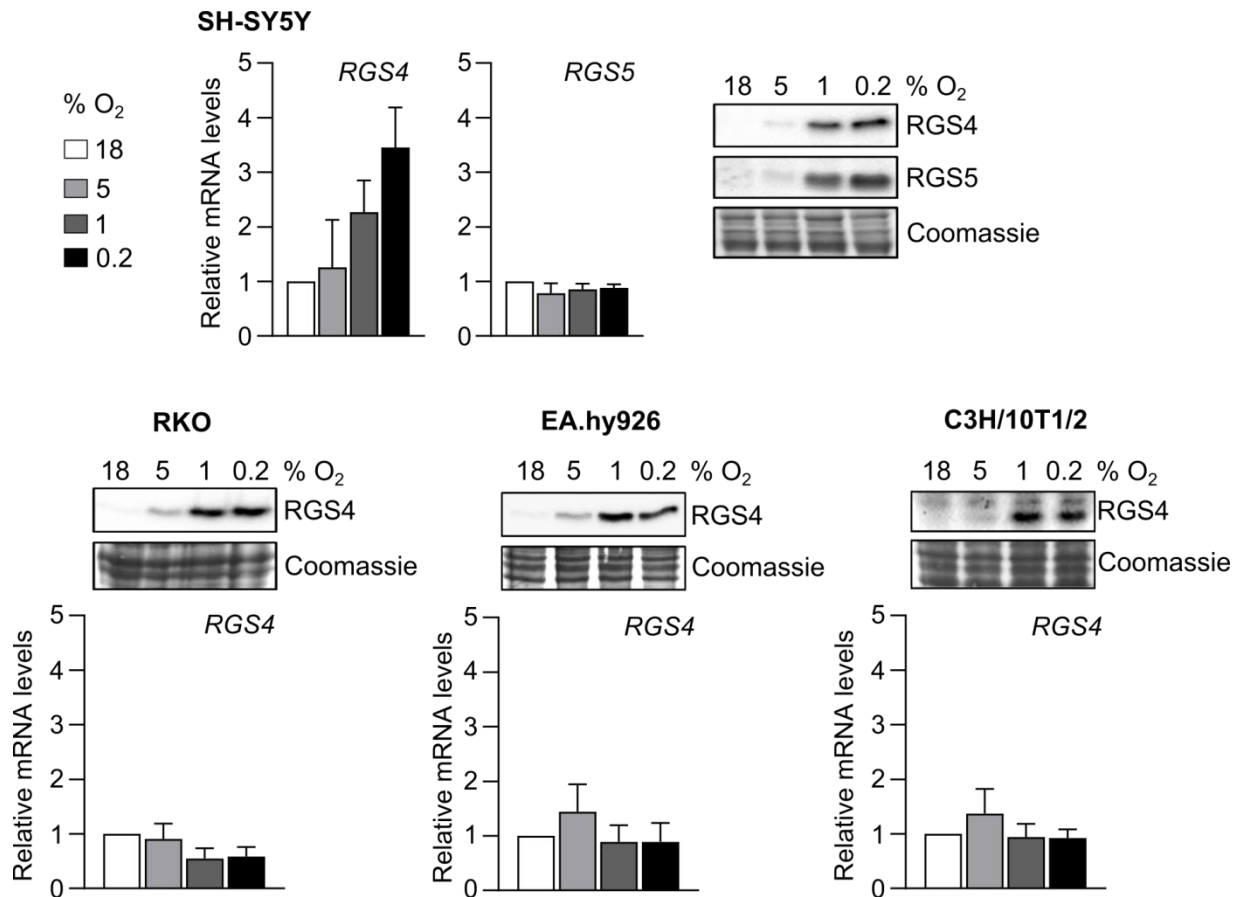


Figure S4. Levels of transcript and protein for RGS4 and RGS5 in human and mouse cell lines exposed to graded hypoxia.

Human SH-SY5Y, RKO and EA.hy926 cells, and mouse C3H/10T1/2 cells were subjected to 5, 1 or 0.2% O₂ for 4 h and lysates collected for analysis of mRNA and protein expression in parallel. Only SH-SY5Y cells exhibited detectable expression of RGS5 protein, whereas all cells expressed RGS4. In SH-SY5Y cells, RGS4 transcript showed induction by hypoxia which was not observed in RKO, EA.hy926 or C3H/10T1/2 cells. In contrast, when expressed at detectable levels, both RGS4 and RGS5 protein increased proportionally to the decline in O₂ in all cell types tested, even in the absence of changes in transcript level. Data are mean \pm S.D. n=3.

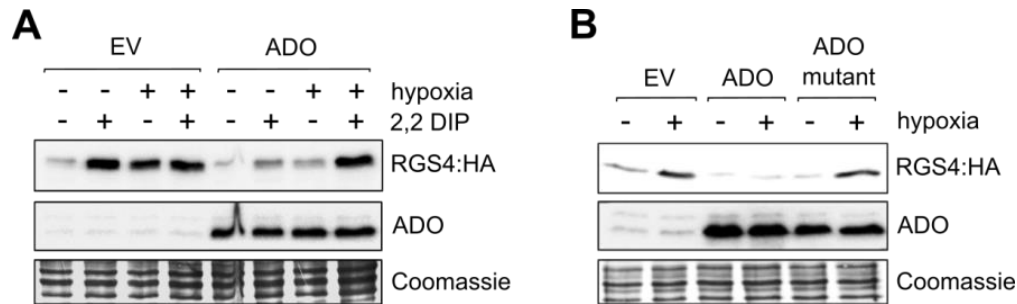


Figure S5. Effect of catalytic inhibition or genetic inactivation of overexpressed ADO on the expression of RGS4:HA.

293T cells were transiently co-transfected with the RGS4:HA reporter, together with empty vector (EV), or vector expressing either WT ADO (ADO) or a catalytically inactive mutant-(H112A, H114A). (A) Transfected cells were exposed to dipyridyl (2,2DIP, 100 μ M) or hypoxia (1% O_2), or both for 16 h. Catalytic inhibition by combined iron chelation and hypoxia was able to overcome the action of overexpressed ADO on RGS4:HA. (B) Genetic inactivation of ADO by a H112A+H114A mutation prevents the ability of overexpressed ADO to suppress hypoxic stabilization of RGS4:HA.

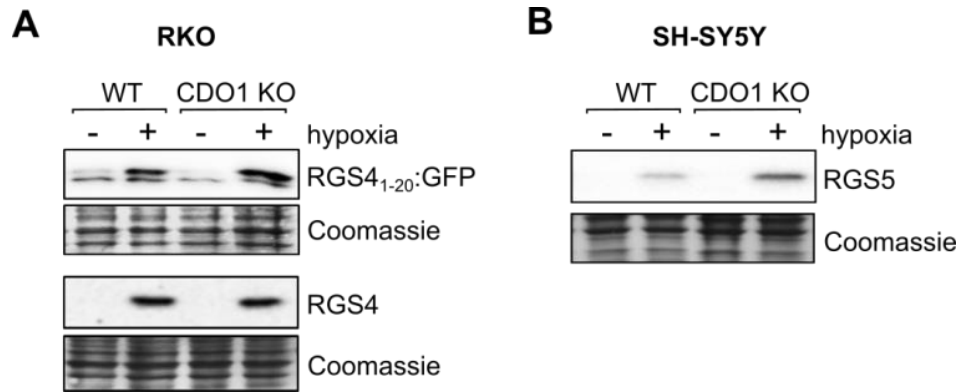


Figure S6. Regulation of RGS proteins by hypoxia in CDO1-deficient cells.

Immunoblots illustrate the up-regulation of RGS4₁₋₂₀:GFP fusion protein together with endogenous RGS4 in and RGS5 by hypoxia (0.1% O₂ for 4h) in CDO1-deficient RKO cells (A) and endogenous RGS5 in CDO1-deficient SH-SY5Y cells (B).

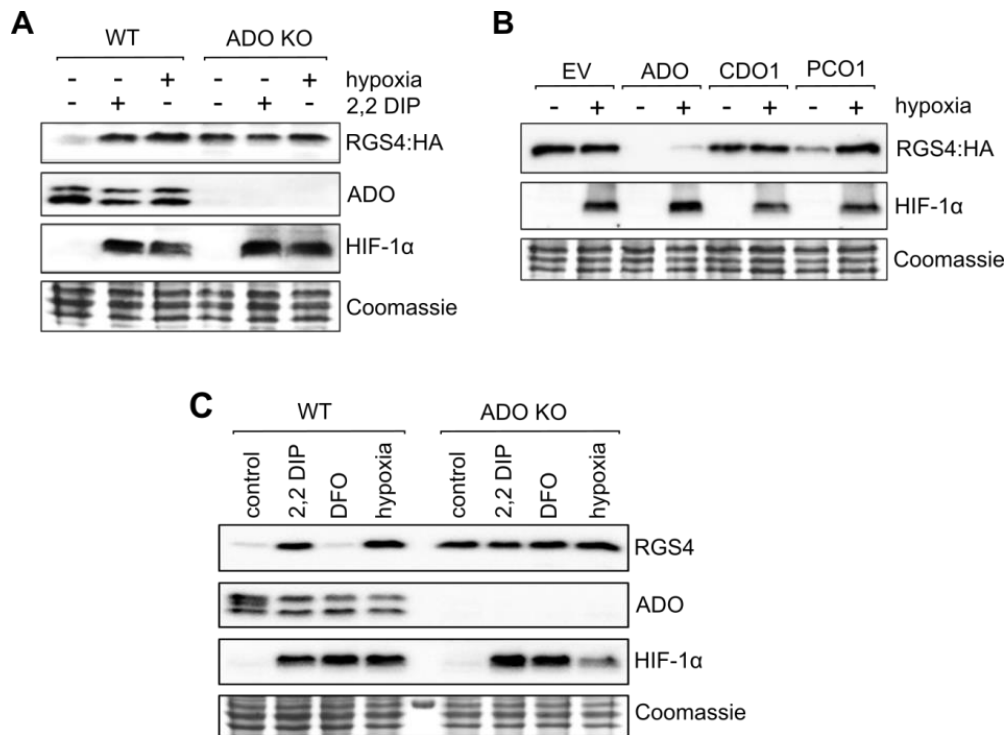


Figure S7. Regulation of RGS4-HA and endogenous RGS4 in ADO-deficient and ADO re-expressing RKO cells.

(A) Immunoblots showing RGS4:HA in wild-type and ADO-deficient RKO cells exposed to hypoxia (0.5% O₂) or dipyridyl (2,2 DIP, 100μM) for 4h. (B) ADO-deficient RKO cells transduced with lentivirus expressing the indicated enzymes or empty vector (EV); ADO and PCO1 repress RGS4:HA and restore regulation by hypoxia, whereas CDO1 has no effect. Similar levels of ADO, CDO1 and PCO1 were verified using parallel immunoblots. HIF-1α immunoblots demonstrate the effect of hypoxia and dipyridyl. (C) Wild-type and ADO-deficient RKO cells exposed to hypoxia, dipyridyl, or desferrioxamine (DFO, 100μM) for 4 h. The response of endogenous RGS4 to these treatments is abrogated in ADO deficient cells.

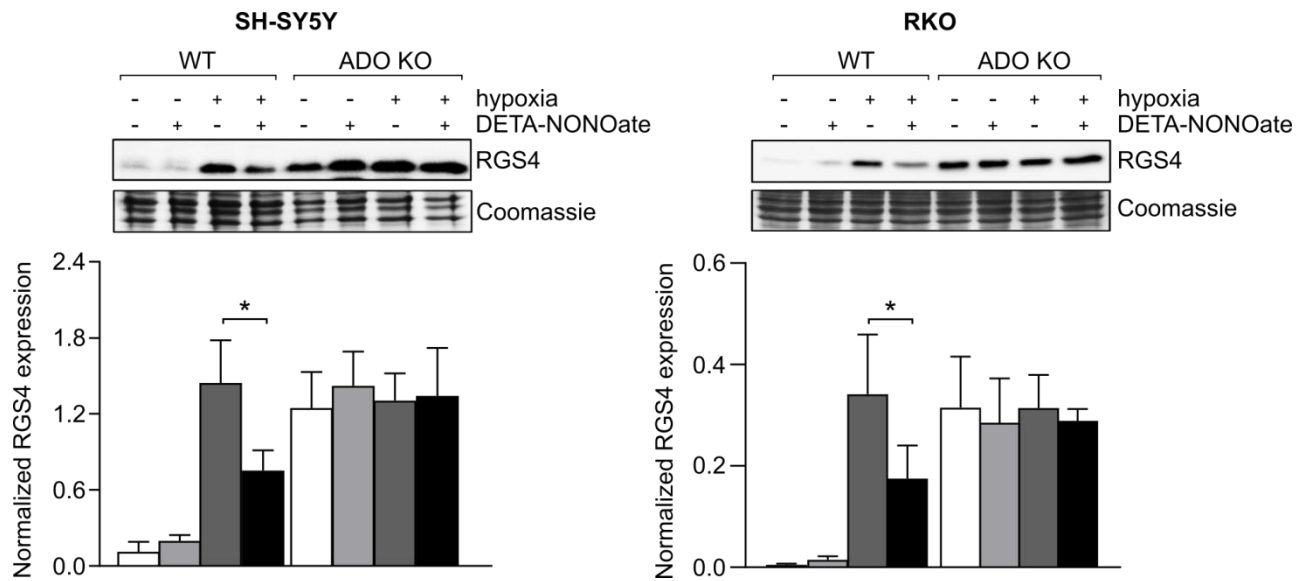


Figure S8. Effect of nitric oxide on RGS4 levels.

Wild-type or ADO-deficient SH-SY5Y and RKO cells were treated with the NO donor 2,2'-(hydroxynitrosohydrazono)bis-ethanimine (DETA NONOate, 100 μ M) for 4 h under normoxic or hypoxic (0.5% O₂) conditions. RGS4 accumulation during hypoxia was attenuated in the presence of NO in wild-type, but not ADO-deficient, cells. Densitometric analysis from three independent blots is shown, with significance assessed by 2-way ANOVA, *p<0.05.

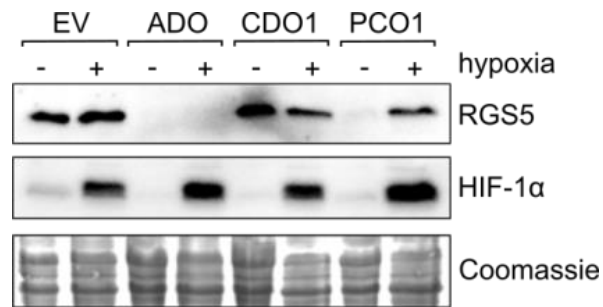


Figure S9. Regulation of RGS5 in ADO-deficient SH-SY5Y cells expressing ADO, CDO1 or PCO1.

Re-expression of ADO and overexpression of PCO1, but not CDO1, in ADO-deficient SH-SY5Y cells suppresses expression of RGS5. Comparable protein levels of each enzyme were verified by immunoblotting. High levels of transfected protein allow ADO, but not PCO1, to overcome effective inhibition by hypoxia. The HIF-1α immunoblot demonstrates that HIF-1 was unaffected by overexpression of these enzymes.

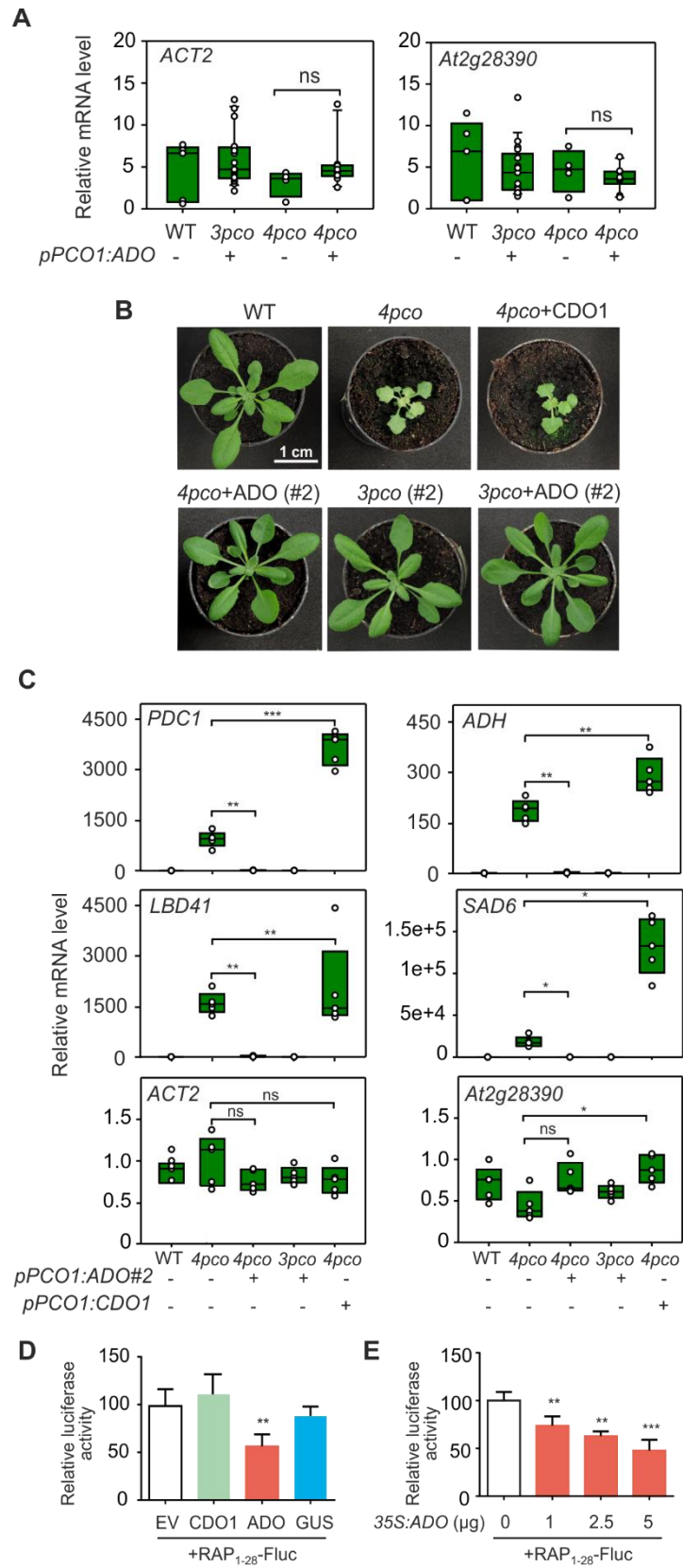


Figure S10. Regulation of plant gene expression and Fluc/Rluc reporter by human ADO and CDO1.

(A) Box plots showing relative mRNA level of *ACT2* and *At2g28390*, two genes whose expression is not affected by ERF-VII activity and hypoxia, in plants corresponding to wild-type *Arabidopsis* plants and *pco* mutants that express human ADO. (B) and (C) In contrast with ADO, expression of human CDO1 did not restore wild-type phenotype (B) and did not counteract the induction of anaerobic genes (*PDC1*, *ADH*, *LBD41* and *SAD6*) (C) in *4pco A. thaliana* mutants; a different *pPCO1:ADO* line from the one shown in Figure 2F was analyzed as an independent control (line #2). Box plots show relative mRNA levels (n=5), asterisks indicate statistically significant difference (* $0.01 < p \leq 0.05$, ** $0.001 < p \leq 0.01$, *** $p < 0.001$) according to the Mann-Whitney Rank Sum Test for *PDC1*, *ADH*, *LBD41* and *SAD6*. A student's t-test was used for *ACT2* and *At2g28390*. (D) ADO, but not CDO1, reduces the stability of a RAP₁₋₂₈-Fluc reporter in transiently transfected mesophyll protoplasts from wild type *A. thaliana*. The unrelated enzyme β -glucuronidase (GUS) was included as a control. Five μ g of each effector plasmid were used, along with 2.5 μ g reporter plasmid. (E) Effect of increasing amount of ADO on RAP₁₋₂₈-Fluc activity. Titration of the ADO effector plasmid is shown. Asterisks indicate statistically significant difference from the control (** $0.001 < p \leq 0.01$, *** $p < 0.001$), according to the Holm-Sidak test.

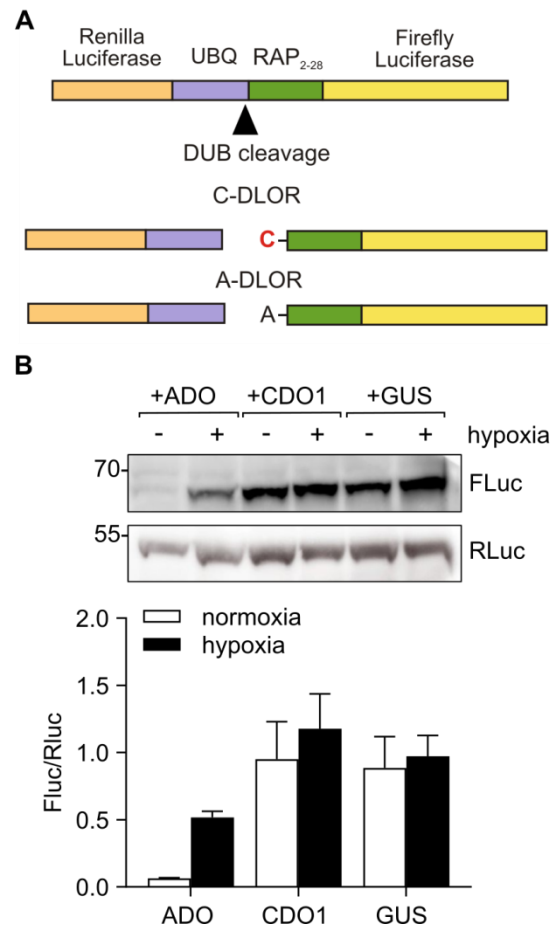


Figure S11. The effects of thiol dioxygenase expression on the RAP2.12-based dual luciferase reporter stability in yeast.

(A) Structure and processing of the Dual Luciferase Oxygen Reporter (DLOR)(29). Deubiquitinating enzymes (DUB) separate *Renilla reniformis* luciferase, fused to a 1-76 fragment of the *Arabidopsis* UBQ1 protein (Q42202-1) (pale purple), from *Photinus pyralis* luciferase, preceded by a 2-28 fragment of the RAP2.12 protein (green) exposing either a Cys, (C-DLOR), or an Ala residue (A-DLOR) at the N-terminus. (B) Representative immunoblots of RAP₂₋₂₈-Fluc and RLuc-UBQ fragments in yeast cells bearing C-DLOR and expressing either vector control (GUS), ADO or CDO1 (confirmed by real time quantitative PCR). (C) Densitometric analysis from two independent experiments. Expression of ADO, but not CDO1, reduces RAP₂₋₂₈-FLuc abundance in *S. cerevisiae* cells in air. Hypoxia corresponds to 6 h treatment at 1% O₂.

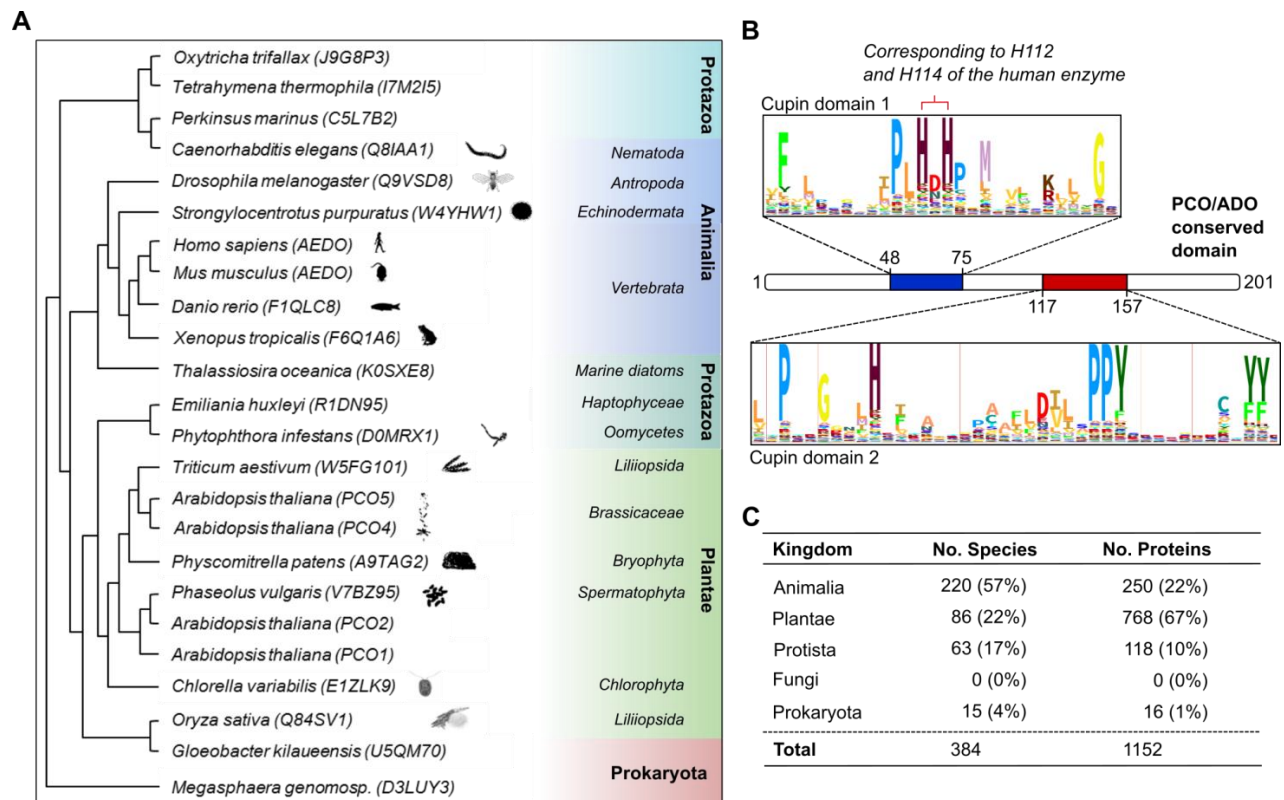


Figure S12. Phylogenetic analysis of PCO/ADO domain containing proteins.

(A) Phylogenetic tree of PCO/ADO domain containing proteins from selected representative species, determined by the Maximum Likelihood method. (B) A graphical illustration of the conserved PCO/ADO domain, determined using a hidden Markov model based on the annotated PCO/ADO domain across all UniProt-verified sequences within the Pfam database (EMBL-EBI). Highest amino-acid conservation was observed within the regions between amino acids 48-75 and 117-157, which conform to the known sequences of cupin domains(15). Residues corresponding to H112 and H114 of the human ADO sequence, mutated to produce a catalytically inactive enzyme in figs. S5 and S17, have been annotated. (C) Summary of the number of species possessing a PCO/ADO-like protein (left column), and the total number of PCO/ADO-like proteins (right column) within each Kingdom, identified within the Pfam database. Numbers in brackets give the percentage of the total number of species/proteins so identified across all Kingdoms, respectively.

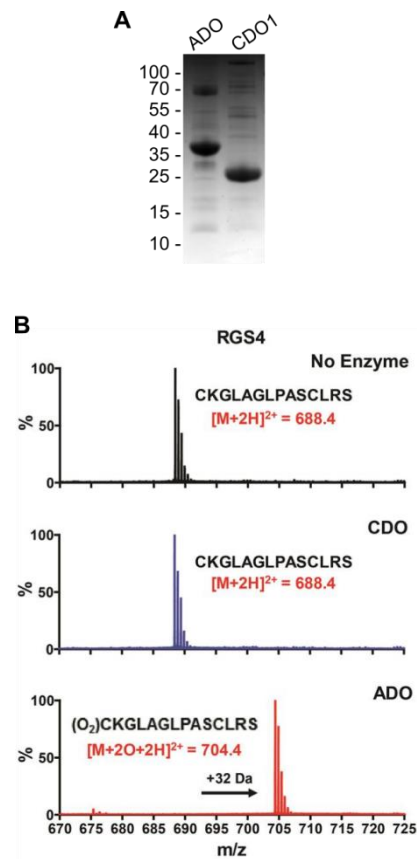


Figure S13. Modification of the RGS4 N-terminal peptide.

(A) Purified recombinant human ADO or CDO1, as used in the described assays, displayed by Coomassie stain following SDS-PAGE (molecular weights indicated in kDa). (B) Mass spectrometry (LC-MS) analyses of the indicated RGS4 N-terminal peptide, incubated aerobically with or without recombinant ADO or CDO1 (1h; 37°C).

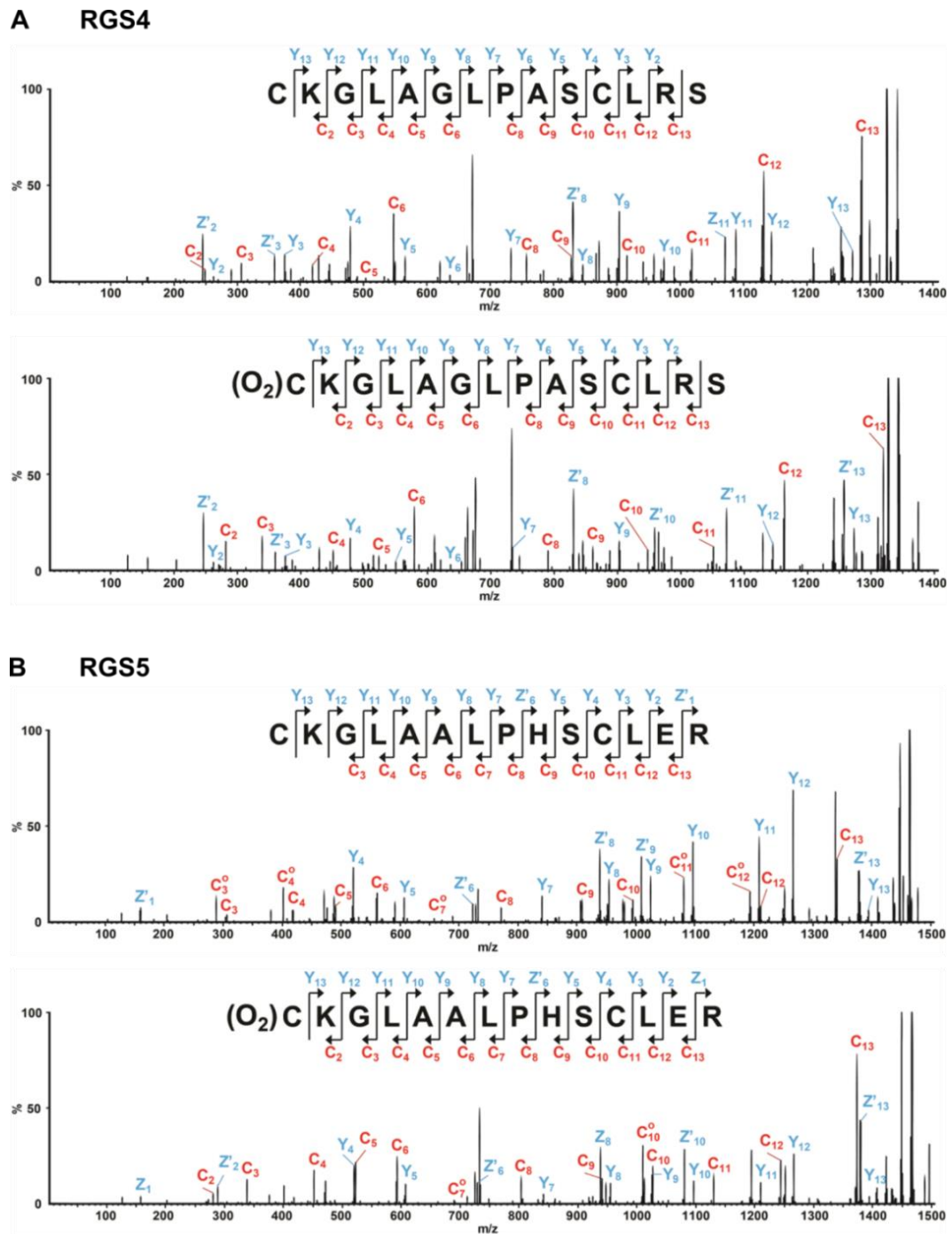


Figure S14. MS² spectra of RGS4 and 5 N-terminal peptides before and after incubation with recombinant ADO.

Fragmentation ion spectra derived from RGS4 (A) and RGS5 (B) N-terminal peptides incubated with (lower panels) or without (upper panels) recombinant ADO. Fragment assignment revealed that in each case incubation with ADO resulted in a mass addition of 32 Da on the N-terminal cysteine.

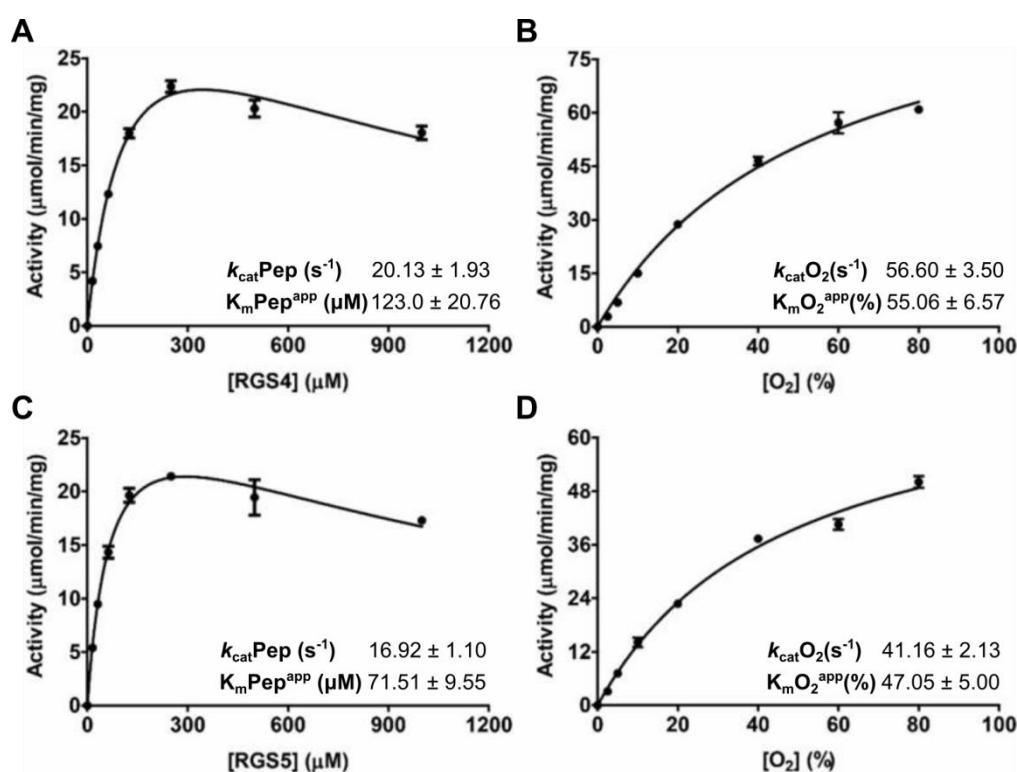


Figure S15. Kinetic analysis of ADO activity with respect to RGS4/RGS5 peptides and O₂.

Michaelis-Menten kinetic plots of ADO activity with respect to the indicated peptide concentration (left panels), and oxygen concentration (right panels). For the activity measurements at different O₂ levels, a peptide concentration was used at which ADO activity was maximal at atmospheric O₂. Data represent mean \pm SEM, n=3.

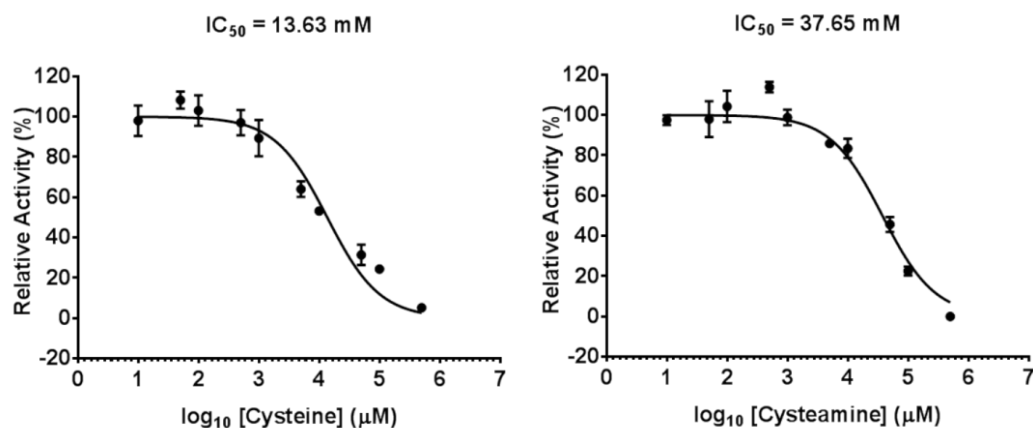


Figure S16. Inhibition of ADO-dependent RGS5 dioxygenation by cysteine and cysteamine.

The effect of free cysteine and cysteamine on the ADO-dependent turnover of RGS5 was determined using a competition assay in which the rate of RGS5 oxidation by ADO was monitored in the presence of different concentrations of cysteine and cysteamine. The data points were normalized to samples measured in the absence of cysteine and cysteamine and plotted to a log inhibitor model versus normalized response model to estimate IC_{50} values. Only high concentrations (mM) of cysteine and cysteamine reduce RGS5 turnover. Data represent mean \pm SEM, $n=3$.

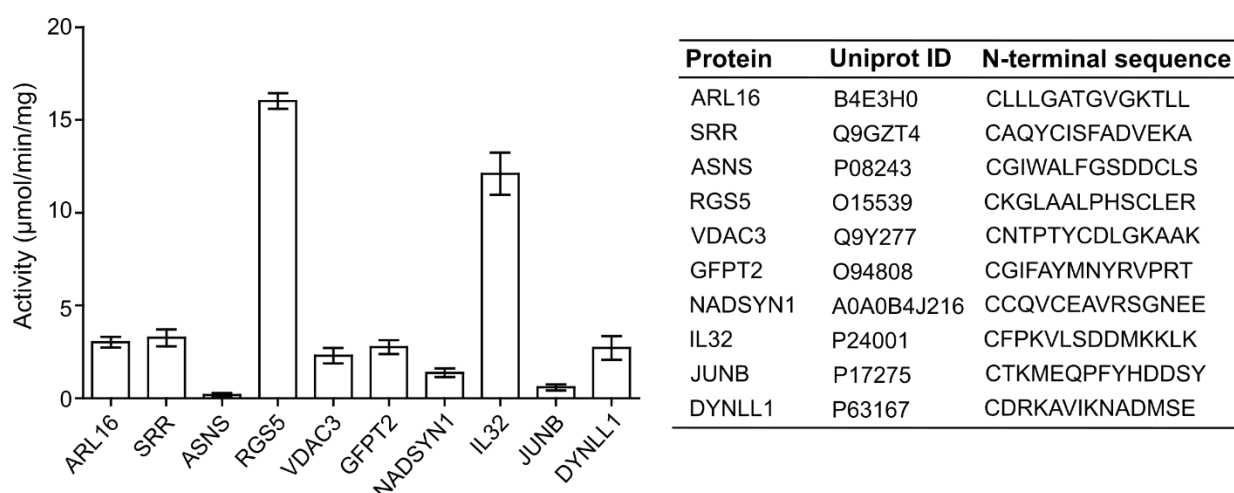


Figure S17. ADO catalytic activity towards candidate mammalian peptides.

14-mer peptides corresponding to the N-termini (Met-cleaved) of the indicated proteins were incubated with recombinant ADO under aerobic conditions at 37°C for 1 min to determine specific activity. Cysteine dioxygenation (UPLC-MS determined mass increase of 32 Da corresponding to the addition of 2 oxygen atoms) was detectable and enzyme-dependent for all tested substrates, though with widely variable rates.

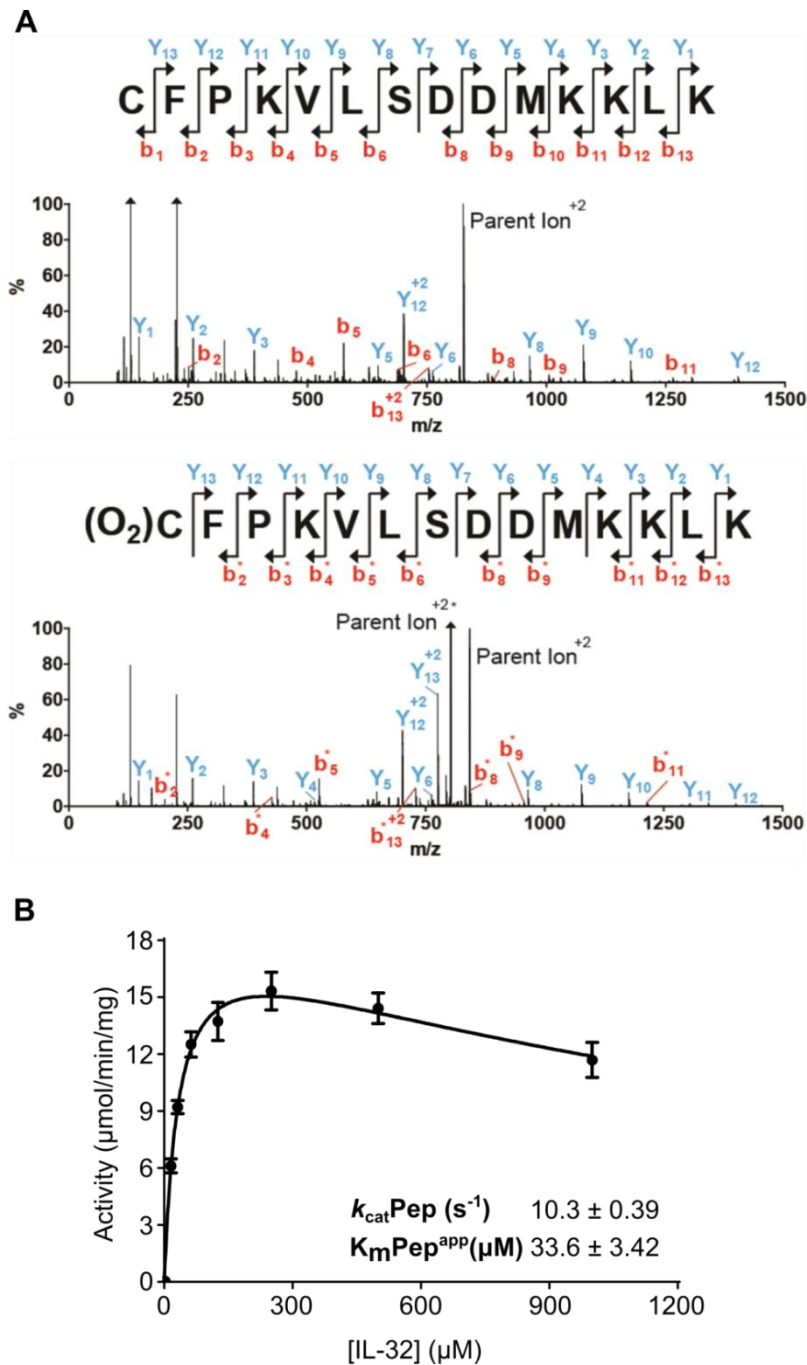


Figure S18. MS² spectra and Michaelis-Menten kinetic plots of an IL-32 N-terminal peptide reacted with ADO.

(A) Fragmentation ion spectra derived from the IL-32 N-terminal peptide incubated with or without recombinant ADO. Fragment assignment revealed that incubation with ADO resulted in a mass addition of +32 Da to the N-terminal cysteine as expected (b* series ions have a consistent -81 Da mass loss likely due to small losses of e.g. SO₂ and NH₃ upon fragmentation; y series ions confirm modification on N-terminal cysteine). (B) Michaelis-Menten kinetic plots of ADO activity with respect to IL-32 peptide concentration, with derived k_{cat} and K_{m} constants listed alongside.

Reference

29. M. L. Puerta *et al.*, A Ratiometric Sensor Based on Plant N-Terminal Degrons Able to Report Oxygen Dynamics in *Saccharomyces cerevisiae*. *J Mol Biol*, (2019).